







# TEFM regulates both transcription elongation and RNA processing in mitochondria

Shan Jiang<sup>1,2</sup> , Camilla Koolmeister<sup>1,2</sup>, Jelena Mistic<sup>1,2</sup>, Stefan Siira<sup>3</sup>, Inge Kühl<sup>4,5</sup> , Eduardo Silva Ramos<sup>4</sup>, Maria Miranda<sup>4</sup> , Min Jiang<sup>4</sup>, Viktor Posse<sup>6</sup>, Oleksandr Lytovchenko<sup>1,2</sup>, Ilian Atanassov<sup>7</sup> , Florian A Schober<sup>2,8</sup>, Rolf Wibom<sup>1,9</sup>, Kjell Hultenby<sup>10</sup>, Dusanka Milenkovic<sup>4</sup>, Claes M Gustafsson<sup>6</sup>, Aleksandra Filipovska<sup>3</sup>  & Nils-Göran Larsson<sup>1,2,4,9,\*</sup> 

## Abstract

Regulation of replication and expression of mitochondrial DNA (mtDNA) is essential for cellular energy conversion via oxidative phosphorylation. The mitochondrial transcription elongation factor (TEFM) has been proposed to regulate the switch between transcription termination for replication primer formation and processive, near genome-length transcription for mtDNA gene expression. Here, we report that *Tefm* is essential for mouse embryogenesis and that levels of promoter-distal mitochondrial transcripts are drastically reduced in conditional *Tefm*-knockout hearts. In contrast, the promoter-proximal transcripts are much increased in *Tefm* knockout mice, but they mostly terminate before the region where the switch from transcription to replication occurs, and consequently, *de novo* mtDNA replication is profoundly reduced. Unexpectedly, deep sequencing of RNA from *Tefm* knockouts revealed accumulation of unprocessed transcripts in addition to defective transcription elongation. Furthermore, a proximity-labeling (BioID) assay showed that TEFM interacts with multiple RNA processing factors. Our data demonstrate that TEFM acts as a general transcription elongation factor, necessary for both gene transcription and replication primer formation, and loss of TEFM affects RNA processing in mammalian mitochondria.

**Keywords** mtDNA replication; RNA processing; transcription elongation

**Subject Categories** RNA Biology; Transcription

**DOI** 10.15252/embr.201948101 | Received 15 March 2019 | Revised 29 March 2019 | Accepted 2 April 2019 | Published online 29 April 2019

**EMBO Reports (2019) 20: e48101**

## Introduction

Mitochondria harbor the oxidative phosphorylation (OXPHOS) system, which performs cellular energy conversion resulting in the production of adenosine triphosphate (ATP) [1,2]. Deficient OXPHOS is a well-established primary cause of mitochondrial disease and is also secondarily implicated in a variety of pathophysiological conditions, such as neurological disease, age-related diseases, and aging [3]. The regulation of OXPHOS is complex because subunits of the respiratory chain and the ATP synthase are encoded by both the nuclear genome and mtDNA [4,5].

Mammalian mtDNA is a gene-dense, circular double-stranded DNA molecule, and the two strands are defined as the heavy (H) and the light (L) strand according to their base composition [6]. The mtDNA only encodes 13 of the ~90 proteins present in the OXPHOS system, but all of these are essential subunits [4,5]. In addition, mtDNA encodes 2 ribosomal RNAs (mt-rRNAs) and 22 transfer RNAs (mt-tRNAs), which are necessary for translation of mitochondrial mRNAs (mt-mRNAs). The compact mtDNA only contains one longer noncoding region named the displacement loop (D-loop), where the origin of replication of the H strand ( $O_H$ ) and the promoters for transcription of H and L strands (HSP and LSP) are located [7,8].

Transcription of mtDNA initiates from HSP and LSP and generates two, near genomic-length polycistronic precursor RNAs, which sequentially go through processing to yield individual mitochondrial RNAs (mtRNAs) [5]. Transcription initiation has been extensively studied using *in vitro* and *in vivo* models, showing that the mitochondrial RNA polymerase (POLRMT) and mitochondrial transcription factors A (TFAM) and B2 (TFB2M) are core components in this process [9–11]. In brief, TFAM unwinds the promoter region of

1 Department of Medical Biochemistry and Biophysics, Karolinska Institutet, Stockholm, Sweden

2 Max Planck Institute Biology of Ageing - Karolinska Institutet Laboratory, Karolinska Institutet, Stockholm, Sweden

3 Harry Perkins Institute of Medical Research and Centre for Medical Research, The University of Western Australia, Perth, WA, Australia

4 Department of Mitochondrial Biology, Max Planck Institute for Biology of Ageing, Cologne, Germany

5 Institute of Integrative Biology of the Cell, UMR9198, CEA, CNRS, University Paris-Sud, Université Paris-Saclay, Gif-sur-Yvette, France

6 Department of Medical Biochemistry and Cell Biology, University of Gothenburg, Gothenburg, Sweden

7 Proteomics Core Facility, Max Planck Institute for Biology of Ageing, Cologne, Germany

8 Department of Molecular Medicine and Surgery, Karolinska Institutet, Stockholm, Sweden

9 Centre for Inherited Metabolic Diseases, Karolinska University Hospital, Stockholm, Sweden

10 Division of Clinical Research Centre, Department of Laboratory Medicine, Karolinska Institutet, Stockholm, Sweden

\*Corresponding author. Tel: +46 8 524 83036; E-mail: nils-goran.larsson@ki.se

double-stranded DNA (dsDNA) and introduces a transcription bubble covering the initiation site. This loose structure is essential for the recruitment of POLRMT and enables TFB2M binding, which completes the assembly of the initiation complex [12,13]. However, once POLRMT successfully transcribes the promoter region, TFB2M is released from the initiation complex [14,15]. Thus, TFB2M is necessary for transcription initiation, but not for elongation. Recent studies have also identified and characterized TEFM as another component of the mitochondrial transcription machinery that interacts with POLRMT and promotes transcription processivity to enable near genome-length transcription [16,17]. The structures of the transcription initiation [18] and elongation complexes [19] have recently been determined. Binding of TEFM to POLRMT allows the complex to form a “sliding clamp” around the DNA, which facilitates high processivity of transcription [19]. TEFM also enhances POLRMT transcription by reducing the duration and frequencies of long-lived transcription pauses [20].

Transcription initiated from LSP also supplies primers for the replication of mtDNA. Using a recombinant *in vitro* transcription system, previous studies have suggested that a large proportion of transcription events initiated at LSP are prematurely terminated at the conserved sequence block II (CSBII) within the D-loop region [21]. This termination occurs because of the formation of a G-quadruplex structure between nascent RNA and the non-template strand of mtDNA and has been proposed to be linked to primer formation for initiation of H-strand DNA replication [22,23]. The newly transcribed RNA remains associated with the CSB region, where it forms an R-loop that is resistant to treatment by RNase A and RNase T1 [24–26]. Interestingly, TEFM has been reported to regulate the generation of replication primers in human mitochondria [27] by helping POLRMT to bypass the highly structured CSBII region [19,20] and abolish R-loop formation [17]. Results from an *in vitro* study have been interpreted to support a model where TEFM serves as a molecular switch that coordinates the balance between mtDNA transcription for replication primer formation and gene expression [27], whereas another *in vitro* study argues that TEFM is a general unspecific transcription elongator needed for mtDNA gene expression [17].

Processing of the newly synthesized polycistronic precursor RNAs to release mature mtRNAs is thought to occur co-transcriptionally and is mainly performed in distinct foci, named mitochondrial RNA granules [28–30]. The RNA granules provide an organizational platform for spatiotemporal regulation of mitochondrial RNA processing and maturation [31]. The majority of mt-rRNAs and mt-mRNAs are flanked by mt-tRNAs and processing starts with the excision of these flanking mt-tRNAs, according to the widely accepted tRNA punctuation model [32]. The endonucleolytic cleavage of the 5'- and 3'-ends of the tRNAs is performed by the mitochondrial RNase P complex, which consists of MRPP1, MRPP2, and MRPP3 [33,34] and the mitochondrial RNase Z (ELAC2) [35,36], respectively, situated in close proximity to the RNA granules [29,37]. The G-rich RNA sequence binding factor 1 (GRSF1) can melt dsRNA [38] and is localized in RNA granules where it interacts with RNase P [29,30]. Other processing factors are also present in the RNA granules, such as the Fas-activated serine/threonine kinase (FASTK) protein family members FASTK, FASTK2 and FASTKD5 [39,40], the mitochondrial poly(A)-polymerase (mtPAP) [41], methyltransferases [42], RNA helicases, and the degradosome (SUPV3L1-PNPase) complex [43].

In this study, we have established the *in vivo* function of TEFM by generating and characterizing conditional *Tefm*-knockout mice. We report that TEFM is essential for embryonic survival and that loss of TEFM in the mouse heart causes mitochondrial cardiomyopathy with severe OXPHOS deficiency. Depletion of TEFM drastically reduces the levels of promoter-distal transcripts encoded by both mtDNA strands. In contrast, there is a marked increase in the steady-state levels of promoter-proximal transcripts at both LSP and HSP in the absence of TEFM. At LSP, these short transcripts are prematurely terminated and shorter than the RNA primers needed for initiation of mtDNA replication. Consistently, *de novo* mtDNA replication is drastically decreased in isolated mitochondria lacking TEFM. Unexpectedly, RNA sequencing (RNA-Seq) and northern blot analyses show that there is an increase of unprocessed mitochondrial transcripts in the absence of TEFM. TEFM proximity-labeling (BioID) assays show that TEFM interacts with diverse RNA processing factors, including the RNase P complex (MRPP1-3), ELAC2, GRSF1, and SUPV3L1-PNPase, which may explain why transcription elongation affects RNA processing. Our results thus show that TEFM is necessary for transcription of mtDNA to generate both short replication primers and near genome-length transcripts for gene expression. Furthermore, we show that loss of TEFM affects both transcription elongation and RNA processing *in vivo*.

## Results

### TEFM is essential for embryonic survival

To determine the *in vivo* function of TEFM, we generated a conditional knockout allele by flanking exon 2 of *Tefm* with loxP sites (Fig 1A). The targeted allele was transmitted through the germline, and heterozygous mice (*Tefm*<sup>+/loxP-puro</sup>) were mated to mice expressing flp-recombinase to excise the puromycin (puro) cassette to obtain mice that were heterozygous for the loxP-flanked *Tefm* allele (*Tefm*<sup>+/loxP</sup>). Heterozygous knockout mice (*Tefm*<sup>+/-</sup>) were obtained by breeding *Tefm*<sup>+/loxP</sup> mice to mice ubiquitously expressing cre-recombinase (+/*β-actin-cre*) (Fig 1A). Intercrossing of *Tefm*<sup>+/-</sup> mice produced no viable homozygous knockout (*Tefm*<sup>-/-</sup>) mice (analyzed offspring, *n* = 94; *Tefm*<sup>+/+</sup>, *n* = 34, *Tefm*<sup>+/-</sup>, *n* = 60 and *Tefm*<sup>-/-</sup>, *n* = 0), demonstrating that loss of *Tefm* results in embryonic lethality. Next, we performed an intercross of *Tefm*<sup>+/-</sup> mice and analyzed staged embryos at embryonic day 8.5 (E8.5; analyzed embryos, *n* = 43). All embryos with the *Tefm*<sup>-/-</sup> genotype (*n* = 11) were small and lacked heart structure, while embryos with the *Tefm*<sup>+/+</sup> (*n* = 10) or *Tefm*<sup>+/-</sup> (*n* = 22) genotype were well developed with normal appearance typical of E8.5 embryos (Fig 1B). Thus, loss of TEFM causes severe developmental defects and embryonic lethality at E8.5, consistent with the phenotype of other knockout mice with homozygous disruption of genes critical for mtDNA expression and maintenance [11,44–46].

### Disruption of *Tefm* in heart leads to cardiomyopathy

Next, we disrupted *Tefm* in heart and skeletal muscle by breeding *Tefm*<sup>+/loxP</sup> mice with transgenic mice expressing cre-recombinase from the muscle creatinine kinase promoter (*Ckmm-cre*).

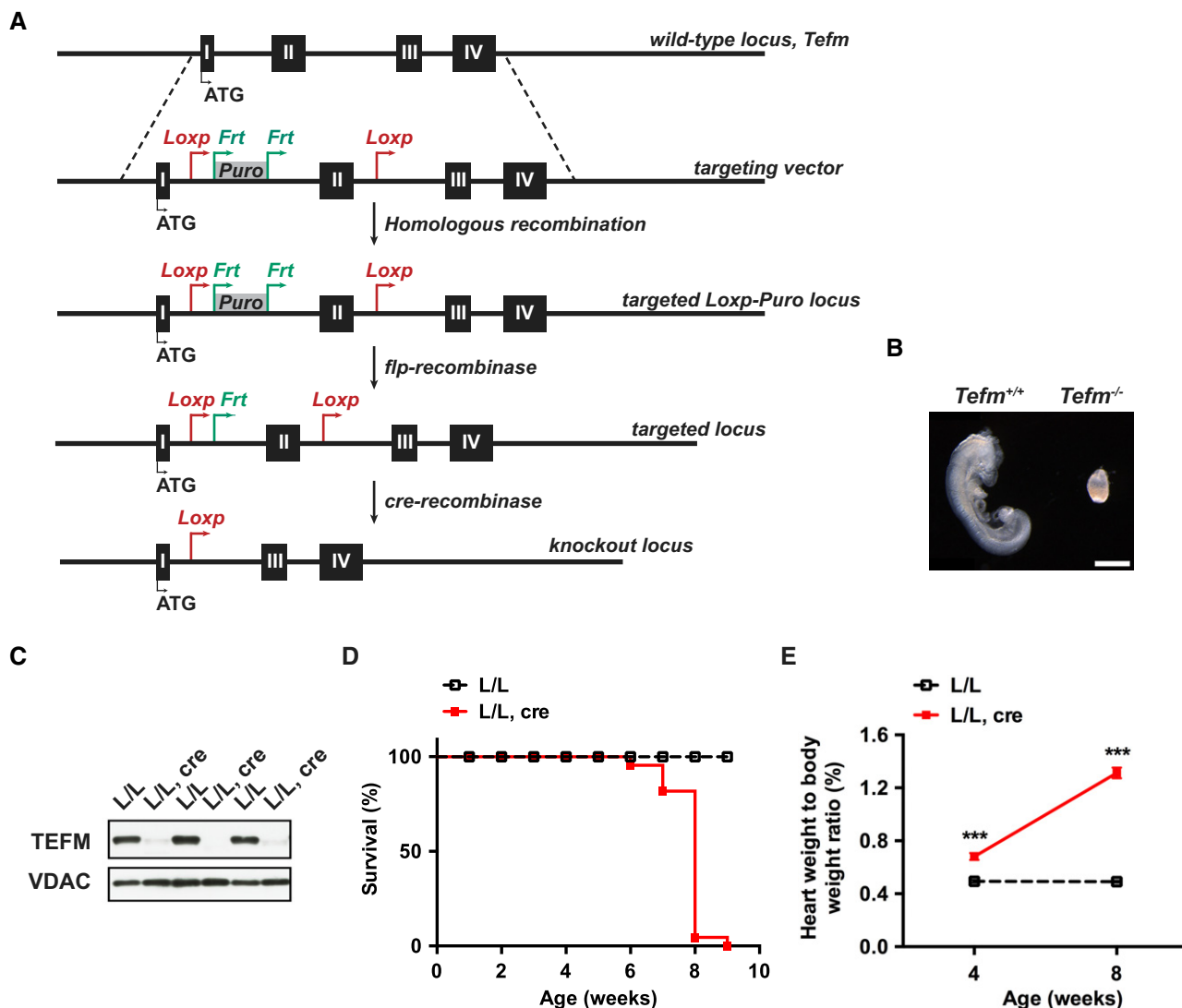


**Figure 1. Disruption of *Tefm* in the germline and heart.**

**A** Targeting strategy for disruption of the *Tefm* gene. *LoxP* sites flanking exon 2 of the *Tefm* gene together with puromycin selection marker (*PuroR*) were inserted into the mouse genome by homologous recombination. The *PuroR* cassette was excised by mating with *flp*-recombinase mice to obtain heterozygous floxed *Tefm* mice (*Tefm*<sup>+/*loxP*</sup>). Whole-body and tissue-specific *Tefm* knockout mice were obtained by crossing *Tefm*<sup>+/*loxP*</sup> with different *cre*-recombinase mice.

**B** Morphology of wild-type (*Tefm*<sup>+/+</sup>) and *Tefm* homozygous knockout (*Tefm*<sup>-/-</sup>) embryos at embryonic day 8.5 (analyzed embryos, n = 43). Scale bar, 500 μm.

**C** Western blot analyses of the TEFM protein level in heart mitochondrial extracts from 8-week-old control (L/L) and tissue-specific *Tefm* knockout (L/L, cre) mice (n = 12 mice for each group). VDAC was used as loading control.

**D** Survival curve for control (L/L; n = 60) and *Tefm* knockout (L/L, cre; n = 22) mice.

**E** Heart weight to body weight ratio in 4- and 8-week-old control (L/L) and tissue-specific *Tefm* knockout mice (L/L, cre). At 4 weeks: L/L n = 22, L/L, cre n = 15; 8 weeks: L/L n = 41, L/L, cre n = 39.

Data information: In (E), data are presented as mean ± SEM. \*\*\*P < 0.001; Student's t-test. 4 weeks P = 5.041476e-009, 8 weeks P = 1.096535e-033.

The tissue-specific *Tefm* knockout mice (*Tefm*<sup>loxP/loxP</sup>, +/*Ckmm-cre*), hereafter denoted *Tefm* knockout mice (L/L, cre), were born at expected Mendelian ratios. The depletion of TEFM in heart was verified at the age of 8 weeks by western blot (Fig 1C) and reverse transcriptase quantitative PCR (RT-qPCR) analyses (Fig EV1A). The *Tefm* knockout mice had a drastically shortened life span with a maximal longevity of 9 weeks (Fig 1D). We also observed a progressively decreased body weight (Fig EV1B) and enlargement of the heart (Fig EV1C–E) in the tissue-specific *Tefm* knockout mice,

resulting in a significant increase in the heart weight to body weight ratio (Fig 1E). TEFM is thus essential for normal heart function.

### Loss of TEFM causes severe mitochondrial dysfunction

Transmission electron microscopy analysis of heart tissue from end-stage knockout mice showed disrupted mitochondrial alignment and disorganized cristae, consistent with severe respiratory chain dysfunction (Fig 2A). Quantification of mitochondrial density

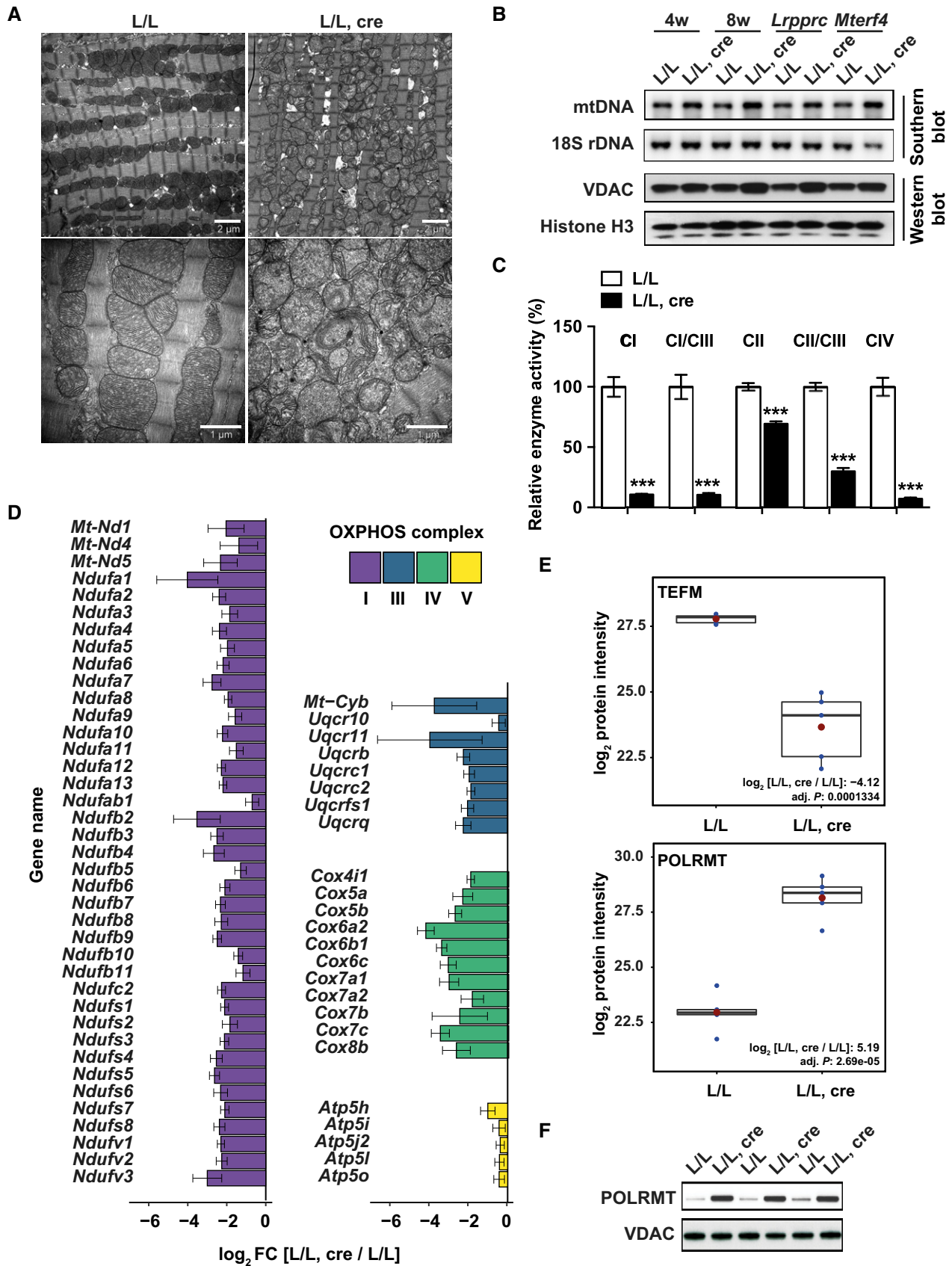


Figure 2.



**Figure 2. Knockout of *Tefm* in heart causes mitochondrial dysfunction.**

- A Transmission electron micrographs of heart tissue in 8-week-old control and *Tefm* knockout mice ( $n = 5$  mice for each group). Scale bar, 2  $\mu\text{m}$  (upper panel) and 1  $\mu\text{m}$  (lower panel).
- B Southern blot analyses of mtDNA levels in control and *Tefm* knockout hearts at the age of 4 and 8 weeks (upper 2 blots;  $n = 6$  mice at each time-point for each group). 18S rDNA was used as loading control. DNA isolated from tissue-specific *Lrprrc* and *Mterf4* knockout hearts used as controls. Western blot analyses of VDAC and histone H3 protein levels in control and *Tefm* knockout hearts at the age of 4 and 8 weeks (bottom 2 blots;  $n = 6$  mice at each time-point for each group). VDAC represents mitochondrial loading, and histone H3 was used as a loading control for nucleus DNA.
- C Respiratory chain complex activities were measured spectrophotometrically and normalized to citrate synthase activity in heart mitochondria from 8-week-old control and *Tefm* knockout mice ( $n = 5$  mice for each group). The analyzed enzyme activities are NADH coenzyme Q reductase (complex I), NADH cytochrome c reductase (complex I/III), succinate dehydrogenase (complex II), and cytochrome c oxidase (complex IV).
- D Barplot of the significantly changed proteins (Benjamini-Hochberg adjusted  $P < 0.05$ ) in *Tefm* knockout mice compared to control mice ( $n = 5$  mice for each group), organized by individual OXPHOS complexes. Proteins are organized in alphabetical order based on gene name.
- E Boxplots of the protein intensity (LFQ) of TEFM (top) and POLRMT (bottom). Red dot: mean; blue dots: intensity value for each biological replicate ( $n = 5$  mice for each group). Horizontal lines: median; box represents the interquartile range (the first quartile (bottom) and third quartile (top) of the intensity value of 5 replicates). The whiskers represent the maximum and minimum values excluding outliers that represent values extend beyond 1.5 times of the interquartile range.
- F Western blot analyses of POLRMT protein levels in control and *Tefm* knockout heart mitochondria at the age of 8 weeks ( $n = 12$  mice for each group). VDAC was used as loading control.

Data information: In (C), data are presented as mean  $\pm$  SEM. \*\*\* $P < 0.001$ ; Student's  $t$ -test. CI  $P = 4.27443\text{E-}06$ , CI/CIII  $P = 2.0553\text{E-}05$ , CII  $P = 2.76012\text{E-}05$ , CII/CIII  $P = 2.00732\text{E-}07$ , CIV  $P = 1.72156\text{E-}06$ . In (D), data are presented as mean ( $\log_2$  [L/L, cre/L/L])  $\pm$  95% confidence interval (CI). In (E), boxplot represents the individual intensity values, the adjusted  $P$ -values are calculated by the moderated  $t$ -test (limma). adj.  $P = 0.0001334$  (top), adj.  $P = 2.69\text{E-}05$  (bottom).

revealed a 1.5-fold increase of relative mitochondrial mass in *Tefm* knockout hearts in comparison with controls (Fig EV2A). We also observed an increased ratio of levels of mtDNA relative to nuclear DNA (18S rDNA) as determined by Southern blot (Fig 2B) and quantitative PCR (qPCR) (Fig EV2B) analyses. Further supporting an activation of mitochondrial biogenesis, we also found an increased ratio of VDAC to histone H3 protein levels as determined by western blots (Fig 2B). This increase of mitochondrial biogenesis typically occurs in severely respiratory chain deficient tissues, as exemplified by analysis of tissue-specific *Lrprrc* knockout and *Mterf4* knockout hearts (Fig 2B) [45,47]. The increase of mitochondrial mass likely represents a compensatory biogenesis response typically seen in human patients and mice with severe mitochondrial dysfunction [48–50]. Next, we measured the activities of the individual complexes in the respiratory chain [51]. We found a drastic decrease in the activity for complexes I, III, and IV in the *Tefm* knockout mice (Fig 2C). A moderate decrease in complex II activity was also observed in the absence of TEFM (Fig 2C), similar to what has been observed in other models with severe reduction of mtDNA expression [52]. Consistently, mitochondrial oxygen consumption assays showed decreased OXPHOS capacity after depletion of TEFM (Fig EV2C and D). Additionally, the expression and the assembly of the respiratory chain complexes were negatively affected as determined by western blot analyses (Fig EV2E) and blue native polyacrylamide gel electrophoresis (BN-PAGE), followed by western blotting (Fig EV2F). Thus, loss of TEFM profoundly impairs OXPHOS, demonstrating that mtDNA transcription elongation is essential for maintaining mitochondrial function.

### Massive changes of the mitochondrial proteome in *Tefm* knockout hearts

To better understand how *Tefm* disruption affects mitochondrial function, purified mitochondria from hearts were subjected to label-free quantitative proteomics. We identified a total of 813 proteins classified as mitochondrial according to MitoCarta 2.0 [53]. Of these, 62.5% (508/813) were significantly changed and showed either increased (338/508) or decreased (170/508) protein levels in mitochondria lacking TEFM. Manual classification of the

differentially expressed proteins revealed that several mitochondrial processes, including oxidative phosphorylation, fatty acid and amino acid metabolic pathways, protein translation (ribosome assembly), mitochondrial structure/morphology, apoptosis, and RNA metabolism, were massively affected by depletion of TEFM (Fig EV3A–C). A closer inspection of the mitochondrial proteome showed a significant decrease of the subunits of OXPHOS complexes I, III, IV, and V (Fig 2D) and increase of respiratory chain complex assembly factors (Fig EV3B). As expected, TEFM protein levels were significantly decreased (Fig 2E). Interestingly, protein levels of nearly all of the small ribosomal subunits (28S) were increased while the majority of the large ribosomal (39S) subunits were decreased (Fig EV3C). These data show that loss of TEFM alters mitochondrial ribosome composition, which may impair mitochondrial protein translation. Furthermore, we observed a remarkable increase of POLRMT protein levels in TEFM-depleted mitochondria (Fig 2E and F), consistent with our previous results showing that knockout of a variety of genes needed for mtDNA expression leads to increased POLRMT levels [54].

### *Tefm* and *Polrmt* double-heterozygous deletion does not affect mitochondrial function or mtDNA transcription

We proceeded to investigate how a moderate reduction of TEFM and/or POLRMT levels affects mitochondrial function and mtDNA transcription. *Tefm*<sup>+/-</sup> mice were crossed with *Polrmt* heterozygous knockout (*Polrmt*<sup>+/-</sup>) mice [11] to generate double-heterozygous knockout mice (*Tefm*<sup>+/-</sup>, *Polrmt*<sup>+/-</sup>). Western blot analyses showed decreased protein levels of TEFM and POLRMT in double-heterozygous knockouts, in accordance with the 50% reduction in *Tefm* and *Polrmt* gene dosage (Fig EV4A). The whole-body reduction of TEFM and POLRMT levels did not lead to any obvious phenotype, and all mice were viable and healthy at the age of 52 weeks. The mtDNA levels were assessed by qPCR at 16 weeks of age and showed no difference between double-heterozygous knockout and control mice (Fig EV4B). Additionally, western blot analyses showed normal levels of the OXPHOS subunits in heart mitochondria from double-heterozygous mice (Fig EV4C), showing that OXPHOS is not affected by a combined moderate decrease of

TEFM and POLRMT levels. Furthermore, northern blot analyses of the steady-state levels of individual mtRNA transcripts, including mt-rRNAs, mt-mRNAs (Fig EV4D and Appendix Fig S1A), and mt-tRNAs (Fig EV4E and Appendix Fig S1B and C), showed no change in double-heterozygous mice in comparison with controls. These data show that a mild reduction in TEFM and POLRMT protein levels does not affect mtDNA expression.

### Loss of TEFM impairs mtDNA transcription elongation and drastically decreases steady-state levels of promoter-distal transcripts

Since TEFM has previously been identified as a component of the mitochondrial transcription machinery *in vitro* [16,17,19], we proceeded to analyze mtRNA transcript levels in hearts from 4- and 8-week-old *Tefm* knockout mice. Northern blot analyses showed a drastic reduction in the steady-state levels of promoter-distal transcripts (mt-rRNAs, mt-mRNAs, and mt-tRNAs) encoded on both strands in the absence of TEFM (Fig 3A–E). In contrast, the levels of promoter-proximal transcripts were either increased, such as mt-tRNA<sup>F</sup> and mt-tRNA<sup>P</sup>, or remained near normal, such as *12S rRNA*, mt-tRNA<sup>V</sup>, and mt-tRNA<sup>E</sup> (Fig 3A–E). The alterations in levels of mt-rRNAs and mt-mRNAs were independently confirmed by RT-qPCR analyses (Fig EV4F). Moreover, the near normal *12S rRNA* levels and decreased *16S rRNA* levels explain the alteration of steady-state levels of mitochondrial proteins found in the mitoproteomics data set (Fig EV3C) and are also consistent with a previous report showing that normal levels of the *12S rRNA* and low levels of *16S rRNA* decrease the levels of large ribosomal subunit proteins, whereas the levels of the small ribosomal subunit proteins remain unaffected [34]. Furthermore, we investigated *de novo* mtRNA synthesis by *in organello* labeling with <sup>32</sup>P-labeled uridine triphosphate (<sup>32</sup>P-UTP) and observed that loss of TEFM led to a dramatically reduced mtRNA levels, predominantly affecting the production of longer transcripts (Fig 4A). Therefore, loss of TEFM impairs mtDNA transcription, particularly transcription elongation, resulting in a severe reduction of promoter-distal transcripts from both strands. The defect in transcription elongation is accompanied by an increase of transcription initiation events, which may also be supported by the increased levels of TFAM and TFB2M (Fig EV4G) and POLRMT (Fig 2E and F), thus leading to drastically increased levels of promoter-proximal transcripts.

### Accumulation of short LSP transcripts in TEFM-deficient mitochondria does not contribute to mtDNA replication

Transcripts initiated from LSP frequently terminate at the conserved sequence blocks (CSBs) resulting in the formation of *7S RNA*, which is the most promoter-proximal L strand transcript [5]. To measure *7S RNA* levels in *Tefm* knockout mice, a <sup>32</sup>P-radiolabeled RNA probe, corresponding to the first 45 base pairs (bp) of the RNA produced by transcription initiation at LSP, was used for northern blot analyses (Fig 4B). Samples from tissue-specific *Mterf4* knockouts, which are known to have increased *7S RNA* levels, and tissue-specific *Polrmt* knockouts, which are known to lack *7S RNA* [11,47], were included as positive and negative controls, respectively. The levels of *7S RNA* were markedly increased in *Tefm* knockout mice in comparison with controls (Fig 4B). The drastically increased abundance of *7S RNA* prompted us to evaluate mtDNA replication, because LSP transcripts are used to prime initiation of mtDNA replication in the CSB region [7,21,55]. Surprisingly, when loaded with equal amounts of mtDNA, the steady-state levels of *7S DNA* within the D-loop were markedly reduced in *Tefm* knockout heart mitochondria (Fig 4C). Furthermore, analysis of *de novo* mtDNA synthesis revealed a drastic reduction in the synthesis of *7S DNA* and full-length mtDNA in the absence of TEFM (Fig 4D). These results show that loss of TEFM impairs mtDNA replication. To address the question why the high levels of *7S RNA* are not associated with increased mtDNA replication, we performed further analysis of the promoter-proximal transcripts using high-resolution polyacrylamide gels (Fig 4E). A range of prematurely terminated RNA species shorter than full-length *7S RNA* were observed in the *Tefm* knockout mice (Fig 4E). The tissue-specific *Mterf4* knockout mice also contain high levels of *7S RNA* reflecting the increase in the rate of transcription in these mice, but in this case the size distribution of *7S RNA* transcripts is the same as in controls without evidence for premature termination. Further analysis with the rapid amplification 3' cDNA ends method (3'RACE) confirmed the findings from the northern blots and showed premature termination of *7S RNAs* (Fig 4F and Table EV1). Promoter-proximal transcription termination for RNA primer formation has been attributed to the G-quadruplex structure of CSBII [22], and it has been reported that TEFM is necessary for reading through this sequence [27]. However, loss of TEFM does not generate a distinct termination product at CSBII, but rather a range of short, prematurely terminated transcripts (Fig 4E and F).

**Figure 3. Loss of TEFM impairs mtDNA transcription elongation and decreases steady-state levels of promoter-distal transcripts.**

A Schematic linear map of mouse mtDNA indicating the relative position of mtRNA transcripts analyzed by northern blot.  
B–E Northern blot analyses (B and D) and relative quantification (C and E) of mtRNA transcripts in control and *Tefm* knockout mouse hearts at the age of 4 and 8 weeks ( $n = 12$  mice at each time-point for each group). *18S rRNA* and *5.8S rRNA* were used as loading controls, respectively.

Data information: In (C and E), data are presented as mean  $\pm$  SEM. \* $P < 0.05$ , \*\* $P < 0.01$ , and \*\*\* $P < 0.001$ ; Student's *t*-test. (C) HSP transcripts: *12S rRNA* 4 weeks  $P = 0.005966044$ , 8 weeks  $P = 0.0806819$ ; *16S rRNA* 4 weeks  $P = 0.000223004$ , 8 weeks  $P = 0.00243443$ ; *Nd1* 4 weeks  $P = 0.0352088$ , 8 weeks  $P = 0.000344158$ ; *Cox1* 4 weeks  $P = 0.000353895$ , 8 weeks  $P = 0.00145773$ ; *Cox2* 4 weeks  $P = 0.0145193$ , 8 weeks  $P = 0.00578484$ ; *Cox3* 4 weeks  $P = 0.00834317$ , 8 weeks  $P = 0.000392364$ ; *Nd5/Cyb* 4 weeks  $P = 0.0010185$ , 8 weeks  $P = 0.00153049$ ; *Nd5* 4 weeks  $P = 0.024621$ , 8 weeks  $P = 7.38074E-05$ ; *Cyb* 4 weeks  $P = 3.46175E-06$ , 8 weeks  $P = 0.000991942$ ; LSP transcript: *Nd6* 4 weeks  $P = 0.000162704$ , 8 weeks  $P = 0.000187855$ . (E) HSP transcripts: *Tf* 4 weeks  $P = 0.0297685$ , 8 weeks  $P = 0.000212544$ ; *Tu* 4 weeks  $P = 0.842023$ , 8 weeks  $P = 0.269231$ ; *Tl1* 4 weeks  $P = 0.00921072$ , 8 weeks  $P = 0.000430068$ ; *Tm* 4 weeks  $P = 0.0084742$ , 8 weeks  $P = 0.000142524$ ; *Tk* 4 weeks  $P = 0.00297015$ , 8 weeks  $P = 0.00010425$ ; *Ts2* 4 weeks  $P = 0.0128829$ , 8 weeks  $P = 2.27321E-05$ ; *Tl2* 4 weeks  $P = 0.00701324$ , 8 weeks  $P = 0.000411549$ ; *Tt* 4 weeks  $P = 0.00572118$ , 8 weeks  $P = 0.000807943$ ; LSP transcript: *Tp* 4 weeks  $P = 0.0427191$ , 8 weeks  $P = 0.0483328$ ; *Te* 4 weeks  $P = 0.464031$ , 8 weeks  $P = 0.13412$ ; *Ts1* 4 weeks  $P = 0.0382215$ , 8 weeks  $P = 0.000478237$ ; *Tc* 4 weeks  $P = 0.00418795$ , 8 weeks  $P = 0.000287525$ ; *Tn* 4 weeks  $P = 0.00531668$ , 8 weeks  $P = 0.000374367$ ; *Ta* 4 weeks  $P = 0.00247257$ , 8 weeks  $P = 0.000564597$ ; *Tq* 4 weeks  $P = 0.00385524$ , 8 weeks  $P = 0.000727981$ .

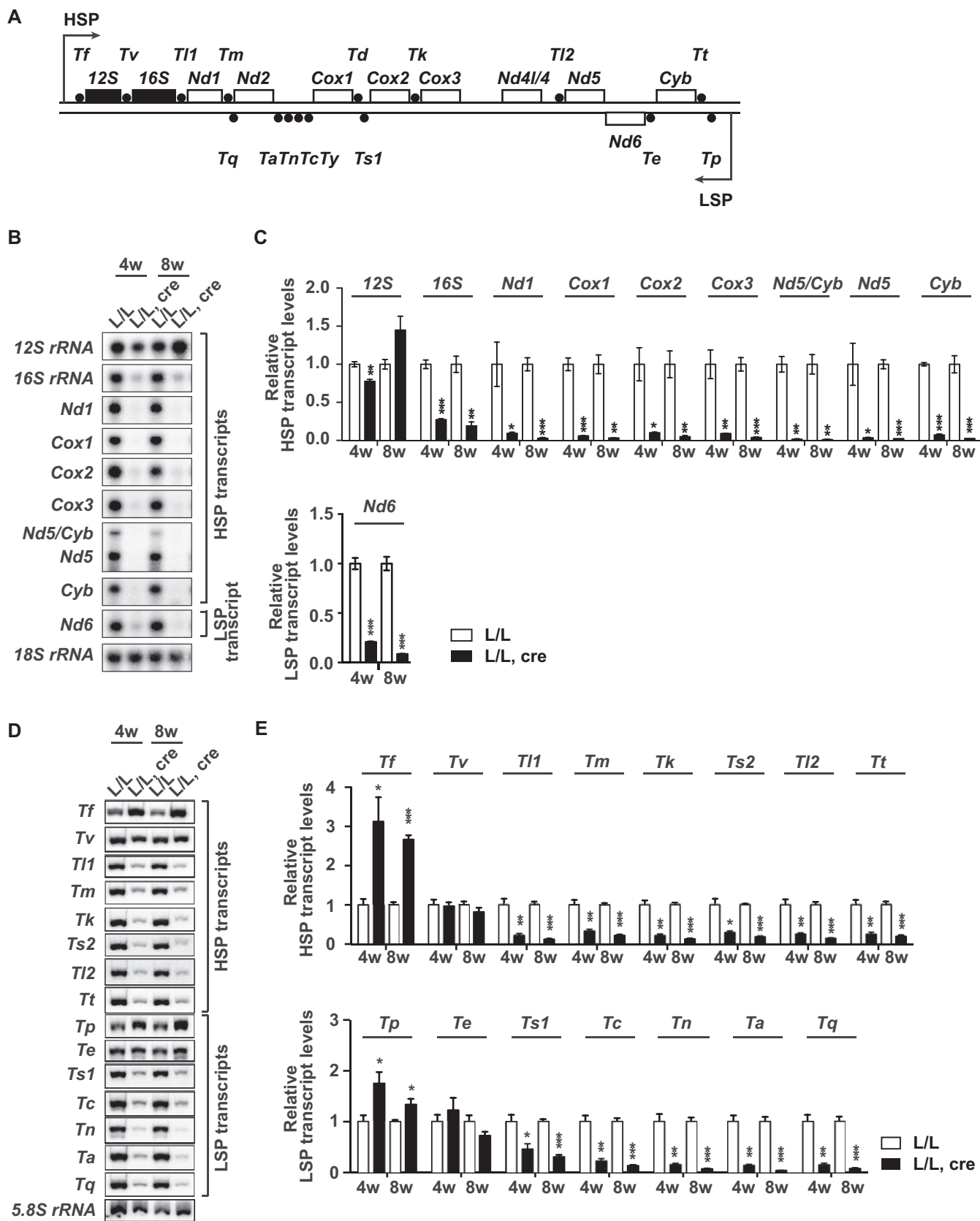


Figure 3.

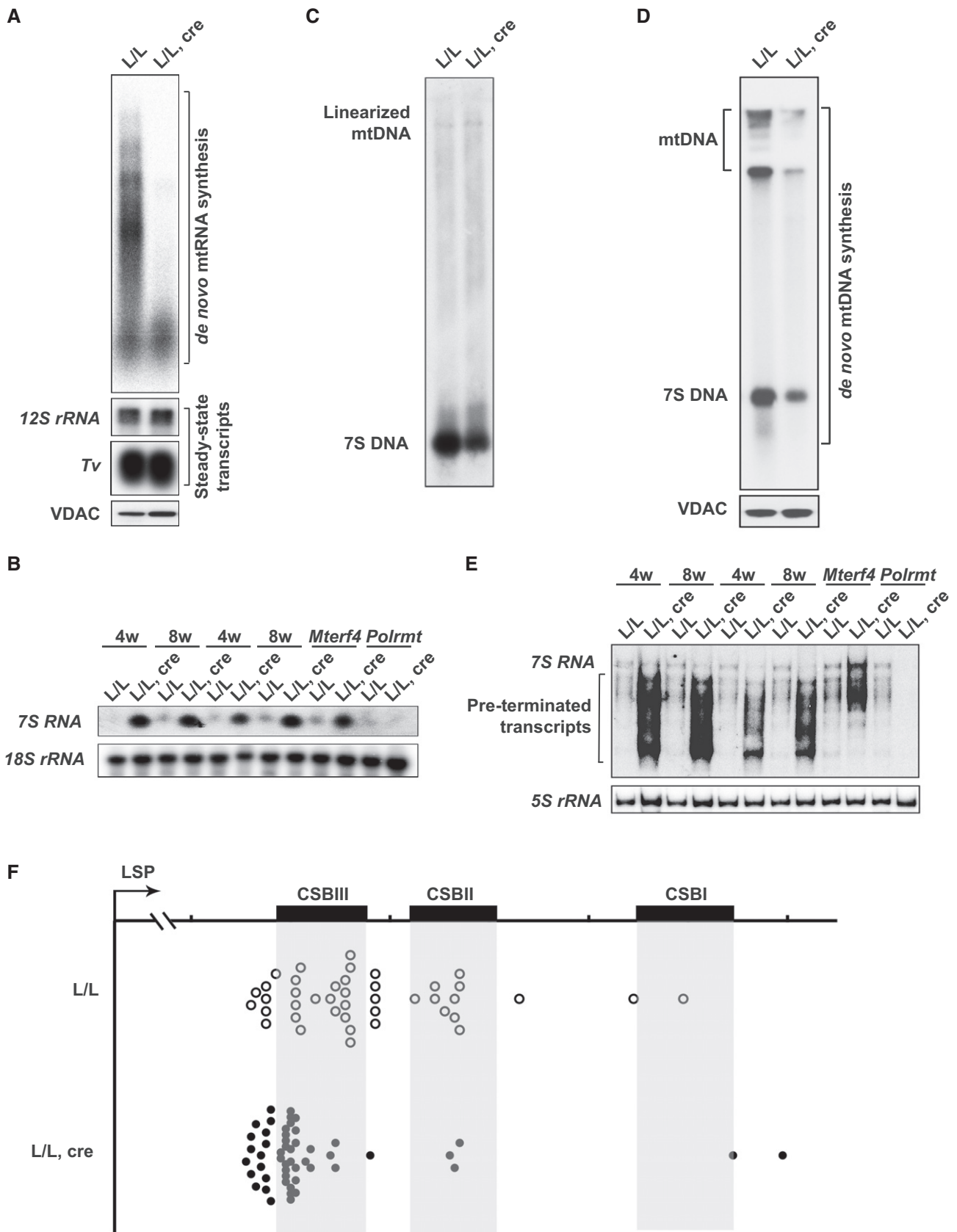


Figure 4.



**Figure 4. Accumulated shorter LSP transcripts in TEFM-depleted mitochondria do not contribute to mtDNA replication.**

- A *In organello* transcription analyses using heart mitochondria isolated from 8-week-old control and *Tefm* knockout mice ( $n = 5$  mice for each group). The steady-state levels of 12S *rRNA* and mt-tRNA<sup>V</sup> were used as endogenous controls, due to their unchanged levels. VDAC was used as loading control for the equal input of mitochondrial extracts. This experiment has performed five times with either two or three replicates.
- B Northern blot analyses of 7S *RNA* level in 4- and 8-week-old control and *Tefm* knockout mouse hearts ( $n = 12$  mice at each time-point for each group). 18S *rRNA* was used as loading control. RNA from tissue-specific *Mterf4* knockout mouse hearts and tissue-specific *Polrmt* knockout mouse hearts was loaded as positive and negative control, respectively.
- C Southern blot analyses of mtDNA to obtain 7S DNA in 8-week-old control and *Tefm* knockout mice. Heart mitochondria from three control or knockout mice were pooled for preparation of mtDNA. Equal amounts of mtDNA shown on the top of the gel were loaded as the endogenous control. This experiment has performed three times.
- D *In organello* replication assays were performed on heart mitochondria isolated from 8-week-old control and *Tefm* knockout mice ( $n = 5$  mice for each group). VDAC was used as loading control.
- E Northern blot analyses of the 7S *RNA* levels in 4- and 8-week-old control and *Tefm* knockout mouse hearts ( $n = 12$  mice for each group). 5S *rRNA* was used as loading control. RNA from tissue-specific *Mterf4* knockout mouse hearts and tissue-specific *Polrmt* knockout mouse hearts was loaded as positive and negative control, respectively.
- F Mapping 3' termini of mitochondrial 7S *RNA*/early LSP transcripts in control (L/L) and *Tefm* knockout (L/L, cre) mouse hearts at the age of 8 weeks. A 3' RACE was performed using linker-ligated RNA and a forward primer corresponding to the first 45 bp from the transcription initiation site at LSP. CSB, conserved sequence block.

We also investigated the expression of core factors involved in mtDNA replication, including the subunit A of the DNA polymerase  $\gamma$  (POL $\gamma$ A), the DNA helicase TWINKLE, and the ssDNA-binding protein (SSBP1) by western blot analyses. We found that POL $\gamma$ A and TWINKLE were significantly increased at the protein level, while SSBP1 expression remained unchanged in TEFM-depleted mitochondria (Fig EV4H). Thus, the defective mtDNA replication capacity does not result from a lack of replication-related proteins. Therefore, our results show that the absence of TEFM causes accumulation of very short, promoter-proximal transcripts initiated from LSP, which prevent proper RNA primer formation to promote mtDNA replication.

#### Transcriptome-wide analysis of RNA from *Tefm* knockout hearts suggests a link between transcription elongation and RNA processing

We further analyzed the mitochondrial transcriptome in total heart tissue and purified mitochondria from *Tefm* knockout and control mice by RNA sequencing (RNA-Seq). We performed TruSeq RNA-Seq, to capture long transcripts, such as mt-mRNAs and mt-rRNAs (Fig 5A and Appendix Fig S2A), and small RNA sequencing to selectively capture mt-tRNAs and the 7S *RNA* (Appendix Fig S2B and C and Fig EV5A). Analyses of both RNA-Seq datasets showed a drastic increase in reads corresponding to promoter-proximal transcripts from both LSP and HSP (e.g., mt-tRNA<sup>F</sup> and mt-tRNA<sup>P</sup>), whereas reads corresponding to promoter-distal transcripts from both strands (16S *rRNA*, all mt-mRNAs and most mt-tRNAs) were decreased (Fig 5A and Appendix Fig S2). These data are consistent with the results from our northern blot and RT-qPCR analyses (Figs 3 and EV4F). The small RNA-Seq dataset revealed the presence of shorter, prematurely terminated transcripts in *Tefm* knockout heart mitochondria (Fig EV5A), which provides independent confirmation of the results shown in Fig 4E and F.

The TruSeq technique only captures mt-tRNAs (or other short RNAs) if they are part of longer, unprocessed transcripts and does not detect free mt-tRNAs [34]. This analysis revealed a marked increase of mt-tRNA reads in the *Tefm* knockout datasets, indicating an accumulation of RNA processing intermediates (Fig 5A). We found that the enrichment of unprocessed transcripts was particularly prominent in regions containing mt-tRNA

clusters or regions spanning tRNA-mRNA junctions (Fig 5A). To further confirm the increase of unprocessed transcripts in *Tefm* knockout mice, we performed strand-specific RT-qPCR (Fig 5B and C). H-strand cDNAs were generated using the anti-mt-tRNA<sup>C</sup>-R primer, which is complementary to the antisense strand relative to mt-tRNA<sup>C</sup>, and the anti-*Nd6*-R primer, which is complementary to the antisense strand of *Nd6*. Synthesis of cDNA with these primers thus generates ssDNA that corresponds to RNAs that are antisense to mt-tRNA<sup>C</sup> and *Nd6*, respectively. In the next step, pairs of primers were used to amplify the cDNA to get dsDNA for analysis by qPCR. As shown in Fig 5B and C, these unprocessed transcripts were upregulated in the absence of TEFM. Moreover, northern blot analyses with a probe corresponding to antisense mt-tRNA<sup>A</sup> confirmed the presence of long unprocessed transcripts in TEFM knockout mice identified by TruSeq (Fig 5D). We thus conclude that absence of TEFM leads to impaired RNA processing.

#### TEFM interacts with RNA processing factors

To further investigate the role of TEFM in RNA processing, we searched for TEFM interacting partners using a proximity-labeling (BioID) assay [56] followed by affinity purification and mass spectrometry of biotinylated proteins. Using Flp-In T-REX 293 cells, we generated a stable cell line that constitutively expressed human TEFM as a fusion protein containing a carboxyterminal BirA\*-HA tag (TEFM-BirA\*). As expected, our results confirmed that TEFM interacts with POLRMT (Fig 6), as previously reported [16,17,19]. In addition, we identified a number of RNA processing-related proteins that interacted with TEFM, including the RNase P complex (MRPP1-3), GRSF1, FASTKD5, ELAC2, mtPAP, and the components of mitochondrial RNA degradosome (SUPV3L1-PNPase) complex (Fig 6), which are all reported to be localized in or adjacent to RNA granules [29,30,37,40,41,57]. Western blot analyses of the eluates confirmed the association between RNA processing factors (ELAC2, GRSF1, and MRPP1) and TEFM (Fig EV5B). As expected, naturally biotinylated proteins, such as carboxylases, were also identified. Furthermore, some very abundant mitochondrial proteins, including respiratory chain subunits, ribosomal proteins, and proteases, were also identified and likely represent the commonly found contaminants, as previously reported in a similar study [58].

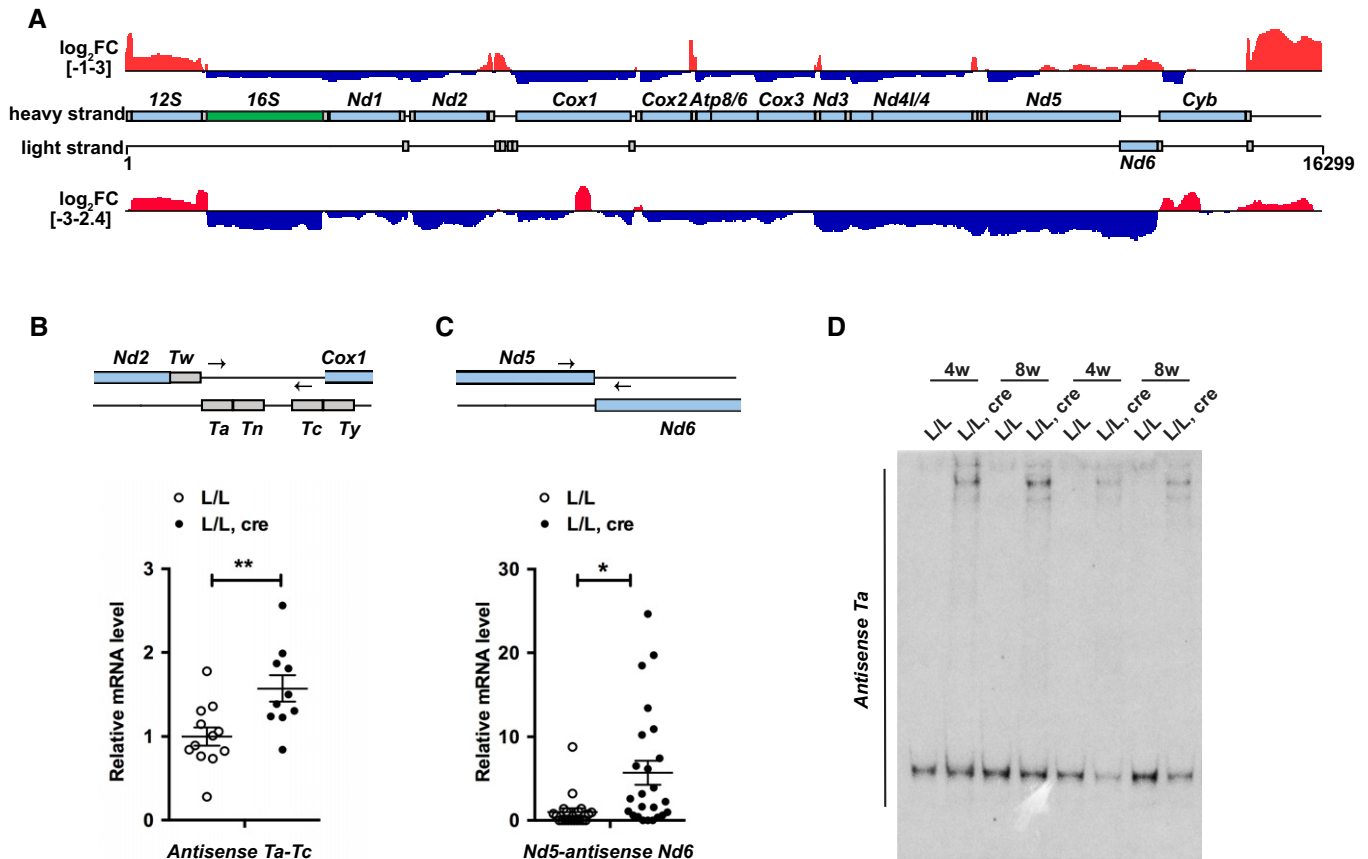


**Figure 5. Transcriptome-wide analysis reveals that mtDNA transcription elongation is linked to RNA processing.**

**A** Transcriptome-wide analysis of the effects of TEFM loss on mtRNA transcripts by TruSeq RNA sequencing. A complete map of mtDNA showing the change in sequence read coverage ( $\log_2$  fold change [L/L, cre/L/L]) between *Tefm* knockout (L/L, cre;  $n = 4$ ) and control (L/L;  $n = 3$ ) mice on both strands. Increased reads are shown in red and decreased reads in blue. The mtDNA is displayed in the central track, with mt-rRNAs in green, mt-mRNAs in light blue and mt-tRNAs in gray.

**B** Strand-specific RT-qPCR detection of the mitochondrial precursor transcripts containing the antisense of mt-tRNA<sup>A</sup> and antisense of mt-tRNA<sup>C</sup> in control and *Tefm* knockout mice ( $n = 12$  mice for each group). The mt-mRNAs are shown in light blue and mt-tRNAs in gray. Arrows show the binding position of qPCR primers. Actin transcript was used as endogenous control.

**C** Strand-specific RT-qPCR detection of the mitochondrial precursor transcripts spanning the junction of *Nd5* and antisense of *Nd6* in control and *Tefm* knockout mice ( $n = 25$  mice for each group). The mt-mRNAs are shown in light blue. Arrows show the binding position of qPCR primers. Actin transcript was used as endogenous control.

**D** Northern blot analyses of the precursor transcripts containing the antisense of mt-tRNA<sup>A</sup> in 4- and 8-week-old control and *Tefm* knockout mouse hearts ( $n = 6$  mice for each group).

Data information: In (B and C), data are presented as mean  $\pm$  SEM. \* $P < 0.05$ , \*\* $P < 0.01$ ; Student's *t*-test. C:  $P = 0.0089$ ; D:  $P = 0.0260$ .

## Discussion

We report here that TEFM acts as a general elongation factor for mtDNA transcription in mammalian mitochondria. Without TEFM, the vast majority of transcripts initiated at LSP does not reach very far and is mostly terminated near CSBIII after initiation. We also report that some regions of mtDNA, such as those with clusters of mt-tRNA genes, seem to be particularly difficult sequences to bypass in the absence of TEFM, likely because of strong secondary structures. Recent computational analyses of the human mtDNA sequence suggest that there are  $\sim 200$  putative G-quadruplex forming sequences [59,60], whose presence has been confirmed in live cells [61]. The existence of G-quadruplexes in the non-transcribed DNA strand constitutes a very strong transcription barrier for a progressing RNA polymerase [62], and a G-quadruplex in nascent

RNA strongly stimulates transcription termination at CSBII [22,23]. It should be noted that the region just upstream of CSBIII is predicted to have the potential to form G-quadruplex by the QGRS mapper, although it has only a modest effect on transcription termination *in vitro* [22]. Clearly, transcription in the absence of TEFM *in vivo* leads to an accumulation of very short transcripts that terminate prematurely and fail to pass through the predicted G-quadruplex at CSBIII.

Unexpectedly, the *in vivo* data we present here also show that loss of TEFM affects RNA processing. By using several independent methods, i.e., RNA-Seq, northern blots, and RT-qPCR, we found abundant, unprocessed transcripts in the absence of TEFM, particularly in regions with strong secondary structures, such as mt-tRNA gene clusters. Label-free quantitative proteomics showed increased levels of many proteins involved in RNA processing in the absence

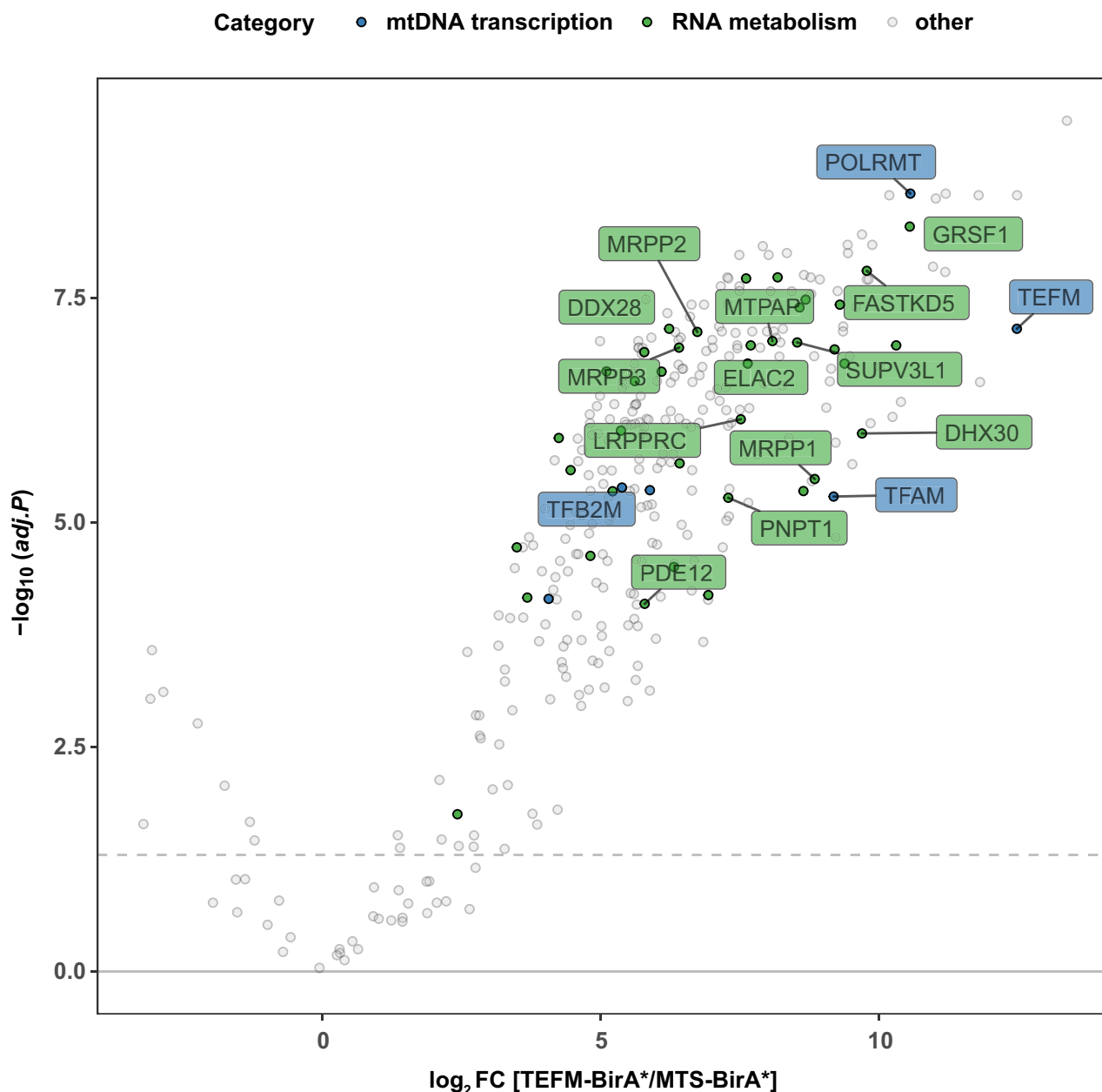


**Figure 6. TEFM interacts with RNA processing factors.**

Volcano plot showing TEFM-BioID. TEFM-BirA<sup>\*</sup>-HA was stably expressed in HEK 293 cells, followed by streptavidin affinity purification and mass spectrometry analysis to detect the associated proteins. Mitochondrial targeted BirA<sup>\*</sup> (MTS-BirA<sup>\*</sup>) was used as a control. The significantly enriched proteins are presented above the horizontal dashed line with 5% false discovery rate (FDR) significance. The blue dots highlight proteins involved in mtDNA transcription, and the green dots represent proteins involved in RNA metabolism. All other proteins are in gray.

of TEFM. By performing BioID assays, we found interactions between TEFM and a range of proteins indispensable for endonucleolytic processing of mtRNAs, e.g., the RNase P complex, ELAC2, and GRSF1. Our results thus suggest that TEFM may interact with the RNA processing machinery in mammalian mitochondria, although further studies are needed to reveal possible molecular mechanisms. A possible coupling between transcription elongation and RNA processing could increase the accuracy and efficiency of pre-RNA maturation and may also provide new regulatory

opportunities to control mtDNA gene expression. It should be pointed out that transcription and pre-mRNA processing are coupled processes also in the nucleus, with important consequences for transcript maturation and gene regulation. In the nucleus, the carboxyl-terminal domain (CTD) of the largest RNA polymerase II subunit is phosphorylated during transcription initiation and this leads to recruitment of proteins involved in RNA processing, including factors required for 5'-capping, splicing, and polyadenylation. By acting as a landing pad that brings processing factors in close

proximity to the actively transcribing RNA polymerase II, the nascent pre-mRNA can be efficiently processed during active transcription elongation. For instance, the nascent pre-mRNA is capped (attachment of 7-methylguanosine by a 5'-5' triphosphate linkage) already after transcription of the first 20–30 nucleotides, just as the 5' end of the nascent transcript emerges from the RNA exit channel [63]. Co-transcriptional processing also helps to explain how chromatin modification, such as histone methylation (H3K36), can mark expressed exons [64]. Future work is needed to reveal additional factors required for co-transcriptional processing in mitochondria and to define their regulatory potential.

Based on results from *in vitro* transcription experiments, previous work suggested that TEFM regulates the formation of the RNA primers needed for initiation of mtDNA replication [27]. This study led to the postulation of a model whereby regulation of TEFM controls a switch between mtDNA gene expression and replication. On the one hand, high levels of TEFM will allow transcription to proceed past CSBII to promote near genome-length transcription for expression of mtDNA-encoded genes. On the other hand, low levels of TEFM will lead to transcription arrest at CSBII and formation of RNA primers needed for mtDNA replication. Data presented here and elsewhere suggest that the mechanisms of primer formation are more complicated than described in the replication–transcription switch model. First, as we show here, loss of TEFM does not lead to an upregulation of mtDNA replication initiation as predicted by the model. Instead, low levels of TEFM cause a drastic decrease in *de novo* mtDNA replication and a depletion of nascent D-loop strands (7S DNA). Second, transcripts formed by premature termination at CSBII cannot be directly used as primers for initiation of mtDNA replication, but must first be processed to shorter transcripts by RNase HI [65]. A role for RNase H in primer maturation has also been reported in other systems. For instance, RNase H is required for R-loop processing and replication primer formation during ColE1 plasmid replication in bacteria [66].

Another interesting finding is that loss of TEFM leads to a dramatic increase of POLRMT levels (Fig 2E and F) and a mild increase of MRPL12 levels (Fig EV3C). One may argue that MRPL12 binds to and stabilizes POLRMT [67,68], but we have failed to confirm this proposed interaction in previous studies [11,54]. In density gradients with wild-type mitochondrial extracts, POLRMT is found in fractions containing mtDNA, whereas MRPL12 is present in mtDNA-free fractions containing other ribosomal proteins [11], arguing against a significant interaction between MRPL12 and POLRMT. Recently, we analyzed the proteome of 5 tissue-specific knockout mouse mutants with disruption of mtDNA gene expression at different levels and found that the expression of 12S and 16S rRNA was critical for the stability of most mitoribosomal proteins [54]. In all of the 5 knockouts, the POLRMT levels were substantially increased (except in the *Polrmt* knockout mice), but the overall levels of mitoribosomal proteins followed the levels of 12S and 16S rRNA. It should be noted that MRPL12 levels were near normal in the absence of 12S and 16S rRNA, but were increased in the two knockouts that can form mitochondrial ribosomes (Fig 5 in [54]). MRPL12 thus belongs to a small subset of mitoribosomal proteins that remains stable in the absence of 12S and 16S rRNA, and the POLRMT protein levels are upregulated independent of changes in MRPL12 levels.

In summary, the *in vivo* results we report here establish TEFM as a crucial component of the mitochondrial transcription machinery. In the absence of TEFM, transcription elongation is severely impaired, resulting in reduced mtDNA expression and a bioenergetics crisis. In contrast to a recently presented model, we find that reduced levels of TEFM do not increase the formation of RNA primers needed for DNA replication. Instead, we show that TEFM is necessary both for replication primer formation and for near genome-length transcription for mtDNA expression. Our *in vivo* results are thus inconsistent with a model where TEFM acts as a switch that regulates the balance between replication and gene expression of mtDNA, and instead, we report a possible connection between transcription elongation to RNA processing that needs to be explained in future molecular studies.

## Materials and Methods

### Experimental model and subject details

#### Mouse models

Generation of conditional *Tefm*-knockout mice. The targeting vector for disruption of *Tefm* in embryonic stem cells (derived from C57BL/6N) was generated by Taconic Artemis using BAC clones from the C57BL/6J RPCIB-731 BAC library. To generate the conditional *Tefm*-knockout allele, exon 2 of the *Tefm* locus was flanked by loxP sites and a puromycin resistance cassette (PuroR) flanked by Frt sites was introduced in intron 1 as a positive selection marker. The PuroR was removed by the mating of *Tefm*<sup>+/loxP-Puro</sup> mice with transgenic mice with ubiquitously expressing flp-recombinase. The resulting *Tefm*<sup>+/loxP</sup> mice were subsequently crossed with mice ubiquitously expressing cre-recombinase under the control of (i) the  $\beta$ -actin promoter (+/ $\beta$ -actin) to generate heterozygous *Tefm* knockout mice (*Tefm*<sup>+/-</sup>) or (ii) the muscle creatinine kinase promoter (+/*Ckmm-cre*) to generate heart and skeletal muscle tissue-specific *Tefm* knockout mice (*Tefm*<sup>loxP/loxP</sup>, +/*Ckmm-cre*; L/L, cre). The *Tefm* and *Polrmt* double-heterozygous knockout mice (*Tefm*<sup>+/-</sup>, *Polrmt*<sup>+/-</sup>) were obtained by intercrossing *Tefm*<sup>+/-</sup> with heterozygous *Polrmt* knockout mice (*Polrmt*<sup>+/-</sup>) [11]. All the mice strains used in this study are listed in Table EV2.

All mice in this study had an inbred C57BL/6N background. Animal studies were approved by the animal welfare ethics committee and performed in compliance with National and European law.

### Method details

#### Morphological analysis

Hearts collected from 8-week-old mice were fixed in 4% paraformaldehyde (PFA) at 4°C for 24 h. Then, the hearts were processed routinely and embedded in paraffin and sectioned to 5  $\mu$ m thickness. Hematoxylin and eosin was performed for structural analysis.

#### Transmission electron microscopy

Left myocardium was cut into small pieces and fixed in 2% glutaraldehyde, 0.5% paraformaldehyde, 0.1 M sodium cacodylate, 0.1 M sucrose, and 3 mM CaCl<sub>2</sub>, pH 7.4 at room temperature for

30 min, followed by 24 h at 4°C. Specimens were rinsed in a buffer containing 0.15 M sodium cacodylate and 3 mM CaCl<sub>2</sub>, pH 7.4; postfixed in 2% osmium tetroxide, 0.07 M sodium cacodylate, 1.5 mM CaCl<sub>2</sub>, pH 7.4 at 4°C for 2 h; dehydrated in ethanol followed by acetone; and embedded in LX-112 (Ladd Research Industries). Ultra-thin sections (40–50 nm) from longitudinal parts were cut and examined in a transmission electron microscope (Tecnai 10; FEI) at 80 kV. Digital images at a final magnification of 8,200× were randomly taken on myofibrils from sections of the myocardium.

#### Crude mitochondrial isolation

Mitochondria from mouse heart were isolated as described previously [49], using mitochondrial isolation buffer (320 mM sucrose, 10 mM Tris-HCl, pH 7.4, and 1 mM EDTA), supplemented with protease inhibitor (Roche) by differential centrifugation. Briefly, hearts were homogenized using Potter-Homogenizer on ice (20 strokes, 500 rpm). Nuclei and cell debris were pelleted at 1,000 g for 10 min at 4°C. Next, the supernatant was centrifuged at 10,000 g for 10 min at 4°C. The differential centrifugation was repeated twice to obtain the crude mitochondria.

#### Western blot analysis

50–100 µg of crude mitochondria were resuspended in 1× NuPAGE™ LDS Sample Buffer. Mitochondrial proteins were then separated by SDS-PAGE (4–12% Bis-Tris Protein Gels; Invitrogen) and transferred onto polyvinylidene difluoride (PVDF) membranes (Merck Millipore). Immunoblotting was performed using standard procedures and developed using ECL reagent. The antibodies used in this study are listed in the Table EV2.

#### RT-qPCR and northern blot analysis

For RT-qPCR, northern blotting, and 3' RACE, total RNA was extracted from heart using Trizol reagent (Invitrogen) according to the manufacturer's instructions and then treated with TURBO DNase-free™ DNase (Invitrogen). For RT-qPCR expression analysis, cDNA was reverse transcribed from 1 µg total RNA using High-Capacity cDNA Reverse Transcription Kit (Invitrogen). The qPCR was performed in a QuantStudio 6 Flex Real-Time PCR System (Life Technologies), using TaqMan™ Universal Master Mix II, with UNG (Applied Biosystems) to quantify mitochondrial transcripts (mt-rRNAs and mt-mRNAs), *Tefm*, *Actin*, and *18S*.

For RT-qPCR detection of transcripts across the tRNA-mRNA junctions, H-strand cDNA was generated by reverse transcriptase PCR using High-Capacity cDNA Reverse Transcription Kit; however, synthesized reverse primers, including Anti-mt-tRNA<sup>C</sup>-R or Anti-*Nd6*-R and *Actin*-R, were used instead of commercial random primers. Then, qPCR was performed using Platinum SYBR Green qPCR supermix-UDG (Invitrogen) to quantify the transcripts containing tRNA-mRNA junctions. Primer pair 1 (mt-tRNA<sup>A</sup>-F and Anti-mt-tRNA<sup>C</sup>-R) was used to detect the antisense transcript of mt-tRNAs cluster on the H strand, shown in Fig 5B. Primer pair 2 (*Nd5*-F and Anti-*Nd6*-R) was used to detect the *Nd5*-antisense *Nd6* junction on the H strand, shown in Fig 5C. *Actin* was used as endogenous control.

For northern blotting, 3 µg of total RNA was separated in either 1% MOPS-formaldehyde agarose gels to detect mt-mRNAs and mt-rRNAs or neutral 10% polyacrylamide gel to detect mt-tRNAs, 7S RNA, and unprocessed mtRNA intermediates. Separated RNAs were

then transferred to Hybond-N+ membranes (GE Healthcare) and hybridized with (i) randomly [<sup>32</sup>P] dCTP-labeled dsDNA probes, following the Prime-It II Random Primer Labeling Kit (Agilent), to detect mt-mRNAs (except *Nd6*), mt-rRNAs, *18S rRNA*, *5S rRNA*, and *5.8S rRNA*; (ii) *in vitro* transcribed single-stranded [<sup>32</sup>P] UTP-labeled RNA probe for *Nd6*, using the Riboprobe Combination System-SP6/T7 RNA Polymerase (Promega); (iii) strand-specific oligonucleotide probes labeled with [<sup>32</sup>P] dATP, using T4 Polynucleotide Kinase (New England Biolabs), to detect mt-tRNAs, 7S RNA, and unprocessed mtRNA intermediates. Radioactive signals were captured in a PhosphorImager screen and was quantified using a Typhoon 7000 FLA and the ImageQuant TL 8.1 software (GE Healthcare). All the Taqman probes and the primer sequences are listed in the Table EV2.

#### 3' RACE

For rapid amplification of 3' cDNA ends (3' RACE), a phosphorylated oligonucleotide linker was first ligated to 2.5 µg of a total RNA using T4 RNA ligase 1 (New England Biolabs). RNA was precipitated and cDNA synthesized using the GeneAmp RNA PCR kit and a primer complementary to the linker sequence (anti-linker). The cDNA was then amplified by PCR using the anti-linker primer and a forward primer corresponding to the first 45 nucleotides from the transcription initiation site at LSP. PCR products were cloned into pCRII-TOPO using TOPO TA Cloning Kit (Invitrogen), following manufacturer's instructions, and direct sequencing of the plasmid from single colonies was performed using M13 forward and M13 reverse primers. Sequence details are listed in Table EV1.

#### DNA isolation and mtDNA quantification

Genomic DNA from mouse heart was isolated with the DNeasy Blood and Tissue Kit (Qiagen) following manufacturer's instructions, followed by treatment with RNase A. mtDNA was measured by quantitative PCR using 5 ng of DNA in a QuantStudio 6 Flex Real-Time PCR System using TaqMan™ Universal Master Mix II, with UNG. The TaqMan assays were used for the detection of mtDNA, which were *Nd1*, *Nd6*, and *Cyb*. *18S* was used to normalize for nuclear input. Three technical replicates were performed.

#### Southern blot analysis and D-loop Southern

For Southern blot analysis, 3 µg of DNA samples was digested with *SacI* to linearize mtDNA molecules, followed by separation on a 0.8% agarose gel and blotted to Hybond-N+ membranes. The D-loop was assessed as described previously [11], and mtDNA was isolated by phenol/chloroform extraction from purified mitochondria. Samples were heated for 3 min at 100°C before loading. Membranes were hybridized with [<sup>32</sup>P] dCTP-labeled dsDNA probes following the Prime-It II Random Primer Labeling Kit to detect total mtDNA (pAM1), the D-loop, or nuclear DNA (18S rDNA) as loading control and exposed to PhosphorImager screens.

#### In organello transcription assay

*In organello* transcription assay was performed on crude mitochondria isolated from mouse hearts. 750 µg of mitochondria was washed three times with 500 µl of cold incubation buffer (25 mM sucrose, 75 mM sorbitol, 100 mM KCl, 10 mM K<sub>2</sub>HPO<sub>4</sub>, 50 µM EDTA, 5 mM MgCl<sub>2</sub>, 1 mM ADP, 10 mM glutamate, 2.5 mM malate, 10 mM Tris-HCl, pH 7.4, and 1 mg/ml BSA). Mitochondria were



pelleted by centrifugation, resuspended in 500  $\mu$ l of transcription labeling buffer supplemented with 40  $\mu$ Ci of [ $^{32}$ P] UTP, and gently rotated for 1 h at 37°C. After incubation, mitochondria were washed with 500  $\mu$ l of washing buffer (10% glycerol, 10 mM Tris-HCl, pH 6.8, and 0.15 mM MgCl<sub>2</sub>) and RNA was isolated with Trizol reagent (Invitrogen), following the manufacturer's instructions. An aliquot of the labeled mitochondria was used for western blot analysis to ensure equal input of mitochondrial extracts. The isolated RNA was analyzed by northern blotting, as described before.

#### *In organello replication assay*

*In organello* replication assay was performed on crude mitochondria isolated from mouse hearts. 750  $\mu$ g of isolated mitochondria was washed three times with 500  $\mu$ l of incubation buffer and resuspended in 500  $\mu$ l of incubation buffer supplemented with 50  $\mu$ M dCTP, 50  $\mu$ M dTTP, 50  $\mu$ M dGTP, and 20  $\mu$ Ci of [ $^{32}$ P] dATP, and incubated for 2 h at 37°C. After incubation, mitochondria were washed three times in washing buffer. An aliquot of the labeled mitochondria was used for western blot analysis to ensure equal input of mitochondrial extracts. Then, mtDNA was isolated by phenol/chloroform extraction using standard procedures, and radio-labeled replicated DNA was analyzed by Southern blotting, as described previously.

#### *Measurement of mitochondrial respiration*

To obtain high-quality crude mitochondria for respiration analysis, heart tissue was finely cut and digested with 0.2% trypsin in 2 ml mitochondrial isolation buffer (310 mM sucrose, 20 mM Tris-HCl, and 1 mM EGTA, pH 7.2) for 10 min at 4°C, with constant rotation. Heart tissue was gently hand-homogenized with 5 ml ice-cold mitochondrial isolation buffer. Mitochondria were purified by differential centrifugation, as previously described. Mitochondrial oxygen consumption flux was measured at 37°C using 25–50  $\mu$ g of crude mitochondria diluted in 2.1 ml mitochondrial respiration buffer (120 mM sucrose, 50 mM KCl, 20 mM Tris-HCl, 4 mM KH<sub>2</sub>PO<sub>4</sub>, 2 mM MgCl<sub>2</sub>, and 1 mM EGTA, pH 7) within an Oxygraph-2k chamber (Oroboros Instruments). The oxygen consumption rate was measured either using 10 mM pyruvate, 10 mM glutamate, and 5 mM malate or 10 mM succinate in the presence of 0.5  $\mu$ M rotenone. The phosphorylating state was obtained using 2.5 mM ADP and the non-phosphorylating state using 125 ng/ml oligomycin. Maximal mitochondrial respiration, uncoupling, was reached by successive addition of CCCP up to 0.3  $\mu$ M.

#### *Blue native polyacrylamide gel electrophoresis*

Crude heart mitochondria (65  $\mu$ g) were solubilized in 16  $\mu$ l of 1 $\times$  NativePAGE sample buffer containing 1% *n*-dodecyl- $\beta$ -D-maltoside (DDM) and incubated on ice for 15 min. Samples were then centrifuged at 20,000 *g* for 30 min at 4°C. Supernatant was collected, and 0.5  $\mu$ l of NativePage 5% G-250 sample additive was added to each sample. Next, proteins and high molecular weight native makers were separated on a 3–12% NativePage gel (Invitrogen) at 120V using a dark blue cathode (1 $\times$  NativePAGE running buffer and 0.5 $\times$  cathode additive) until the blue-front migrated 50% of the gel followed by a light blue cathode buffer (1 $\times$  NativePAGE running buffer and 0.1 $\times$  cathode additive). The anode buffer consisted of 1 $\times$  NativePAGE running buffer. For western blot analysis, proteins were then blotted onto a PVDF membrane with transfer buffer

(48 mM Tris and 39 mM glycine) for 1.5 h at 400 mA. Membranes were completely destained with methanol before proceeding with standard immunoblotting.

#### *Ultrapure mitochondria isolation*

Ultrapure mitochondria were prepared as previously described [54]. Crude mitochondrial pellets from mouse hearts were washed in 1 $\times$ M buffer (220 mM mannitol, 70 mM sucrose, 5 mM HEPES pH 7.4, 1 mM EGTA pH 7.4); pH was adjusted with potassium hydroxide, supplemented with EDTA-free complete protease inhibitor cocktail and PhosSTOP Tablets (Roche), and purified on a Percoll density gradient (12%:19%:40% prepared with buffer 2 $\times$ M) via centrifugation in a SW41 rotor at 41,086 *g* at 4°C for 1 h in a Beckman Coulter Optima L-100 XP ultracentrifuge using 14  $\times$  89 mm Ultra-Clear Centrifuge Tubes (Beckman Instruments Inc.). Mitochondria were harvested at the interphase between 19 and 40%, and washed three times with buffer 1 $\times$ M, and mitochondrial pellets were frozen at –80°C. Purified frozen mitochondria pellets were suspended in lysis buffer (6 M guanidinium chloride, 10 mM Tris(2-carboxyethyl)phosphine hydrochloride, 40 mM chloroacetamide, and 100 mM Tris-HCl). After complete lysis, samples were diluted 1:10 in 20 mM Tris-HCl pH 8.0 and 80  $\mu$ g of protein was mixed with 3  $\mu$ g of Trypsin gold (Promega) and incubated overnight at 37°C to achieve complete digestion. Peptides were cleaned with home-made STAGetips [69] (Empore Octadecyl C18; 3M) and eluted in 60% acetonitrile/0.1% formic acid buffer. Samples were dried in a SpeedVac apparatus (Eppendorf concentrator plus 5305) at 45°C, and the peptides were suspended with 0.1% formic acid. Approximately 1.5  $\mu$ g of peptides was analyzed by LC-MS/MS.

#### *Label-free quantitative proteomics*

Peptides were separated on a 25 cm, 75  $\mu$ m internal diameter Pico-Frit analytical column (New Objective) packed with 1.9  $\mu$ m ReproSil-Pur media (Dr. Maisch) using an EASY-nLC 1200 (Thermo Fisher Scientific). The column was maintained at 50°C. Buffer A was 0.1% formic acid in water; buffer B was 80% acetonitrile, 0.1% formic acid. Peptides were separated on a segmented gradient from 3 to 6% buffer B for 10 min, from 6 to 25% buffer B for 100 min, from 25 to 31% buffer B for 10 min, and from 31 to 60% buffer B for 10 min, at 200 nl/min. For the BioID experiment, peptides were separated on a segmented gradient from 6 to 31% buffer B for 80 min and from 31 to 50% buffer B for 10 min. Eluting peptides were analyzed on a QExactive HF mass spectrometer (mitoproteome quantification, Thermo Fisher Scientific) or Orbitrap Fusion (BioID experiment, Thermo Fisher Scientific). Peptide precursor mass to charge ratio (*m/z*) measurements (MS1) was carried out at 60,000 $\times$  resolution, in the 300–1,800 *m/z* range. The top ten most intense precursors with charge state from 2 to 7 only were selected for HCD fragmentation using 25% normalized collision energy. The *m/z* of the peptide fragments (MS2) was measured at 30,000 $\times$  resolution, using an AGC target of 2e5 and 80-ms maximum injection time. Upon fragmentation, precursors were put on an exclusion list for 45 s.

#### *BioID*

TEFM-BirA\*-HA and MTS-BirA\*-HA (mitochondrial targeting sequence from human COX8a) were cloned into pcDNA5/FRT/TO

vector. Human Flp-In T-REx 293 cells were nucleofected using Nucleofector™ Lonza device. Cells were seeded in DMEM GlutaMax and supplemented with 10% FBS and 1% pen/strep (100 U/ml). The next day, 200,000 cells were collected and resuspended in 20  $\mu$ l of Nucleofector™ Solution with 900 ng of pOG44 and 100 ng of construct. 24 h after nucleofection, cells were passaged into 10-cm<sup>2</sup> plates and selected by the addition of hygromycin and blasticidin at final concentration of 100 and 10  $\mu$ g/ml, respectively. This selection medium was changed every 2–3 days until clear visible colonies were present. Several colonies per construct were picked and expanded. Selected clones were scaled up to one 245  $\times$  245  $\times$  25 mm<sup>3</sup> square dish for treatment and harvesting. The cells were induced with 1  $\mu$ g/ $\mu$ l of doxycycline at around 70% of confluency. The day after, cells were treated with 50  $\mu$ M biotin for protein labeling. Cells were harvested 24 h later and washed three times with PBS by pelleting at 800 g for 5 min at 4°C. Mitochondria were isolated using mitochondria isolation buffer (20 mM HEPES pH 7.6, 220 mM mannitol, 70 mM sucrose, 1 mM EDTA, 1 $\times$  protease inhibitor, 2 mg/ml BSA) by differential centrifugation. The cells were homogenized in homogenizer by applying 15–20 strokes. This suspension was then centrifuged at 800 g for 5 min at 4°C. Collected supernatant was centrifuged at 10,000 g for 10 min at 4°C. Pellet (crude mitochondria) was then resuspended in mitochondria isolation buffer without BSA and centrifuged again at 10,000 g for 10 min at 4°C.

Pull-down experiments were performed according to the published protocol [56] with small modifications. Mitochondrial pellet was lysed in 1 ml of lysis buffer (50 mM Tris-HCl, pH 7.4, 500 mM NaCl, 0.2% SDS, 1 $\times$  protease inhibitor, 1 mM DTT). Subsequently, 20  $\mu$ l of 20% Triton X-100 was added. Samples were incubated for 30 min on ice and then centrifuged at 16,500 g, 4°C for 10 min. Dynabeads MyOne Streptavidin C1 (Thermo Fisher Scientific) were incubated with the lysates on a rotator at 4°C overnight. There were 9 following washing steps. Samples were eluted in elution buffer (2 M Urea, 5 ng/ $\mu$ l Trypsin, 1 mM TCEP, 50 mM Tris-HCl, pH 7.5) at room temperature. A volume of 5 mM CAA was added to the samples, and reaction was incubated at 37°C overnight. The samples were further analyzed by LC-MS/MS mass spectrometry. The proteins of TEFM-BioID are listed in Dataset EV1.

#### LC-MS/MS data analysis

The raw data were analyzed with MaxQuant [70] version 1.5.2.8 using the integrated Andromeda search engine [71]. Peptide fragmentation spectra were searched against the canonical and isoform sequences of the mouse reference proteome (proteome ID UP000000589, downloaded August 2015) or the human reference proteome (BioID experiment, proteome ID UP0000005640, downloaded September 2018) from UniProt. The database was automatically complemented with sequences of contaminating proteins by MaxQuant. Methionine oxidation and protein N-terminal acetylation were set as variable modifications. Digestion parameters were set to “specific” and “Trypsin/P”, allowing for cleavage after lysine and arginine, also when followed by proline. The minimum number of peptides and razor peptides for protein identification was 1; the minimum number of unique peptides was 0. Protein identification was performed at a peptide spectrum matches and protein false discovery rate of 0.01. The “second peptide” option was on to identify co-fragmented peptides. Successful identifications were

transferred between the different raw files using the “Match between runs” option, using a match time window of 0.7 min. Label-free quantification (LFQ) [72] was performed using an LFQ minimum ratio count of 2.

Analysis of the label-free quantification results was performed with Perseus computation platform [73], version 1.5.0.0 and R [74]. Proteins marked as “Reverse”, “Only identified by site”, and “Potential contaminant” were removed. LFQ intensity values were log<sub>2</sub> transformed and proteins that contained at least three valid values in L/L or L/L, cre groups, and five valid values for the BioID experiment were kept for further analysis.

Missing values were imputed with a width of 0.3 and down shift of 1.8. Differential expression analysis was performed using the two-sided moderated *t*-test from the limma package [75]. Proteins with a Benjamini-Hochberg adjusted *P* < 0.05 were designated as differentially regulated. Differentially expressed proteins were manually classified into selected mitochondrial pathways.

#### RNA sequencing analyses

RNA was isolated from total mouse heart and crude heart mitochondria using the miRNeasy Mini Kit (Qiagen), according to manufacturer’s instructions. RNA quantity, purity, and integrity were verified using a Bioanalyzer.

**TruSeq library analysis** Sequenced reads were aligned to the mouse genome reference sequence (mm10), masked for NUMTs regions, with bowtie2 v2.2.9 [76], and the subsequent alignments filtered with SAMtools v1.3.1 [77] (-q 2 -f 2 -F 256) to retain mapped proper pairs and exclude secondary alignments and multireads (read alignments with equal primary and secondary alignment scores). Mitochondrial alignments were extracted, split by template strand, and converted to full-length RNA fragment BED files, before coverage was calculated with BEDtools [78] genomcov (-d -scale [1e+06/total mapped reads]), normalized to the total number of fragments mapped to the mouse whole genome (reads per million; RPM), and converted to wig format for visualization. Gene-level counts for the nuclear genome were calculated with featureCounts [79] (-s 2) using the GENCODE vM12 annotation (excluding mitochondrial annotations), while counts for mitochondrial genes were calculated with BEDtools coverage (-counts -s -F 0.80) using a GENCODE-based annotation with contiguous mt-Atp8/6 and mt-Nd4 l/4 intervals, and an approximate 7S RNA annotation (chrM:16035-16188). BEDtools coverage was used for mitochondrial genes due to their compact genomic organization and the subsequent overlapping of multiple genes by read alignments with post-transcriptional 5’ or 3’ extensions, which is addressed by specifying a minimum 80% overlap between the read and the annotation. Count tables were collated in R v3.3.2 [74], and differential expression between conditions was analyzed with DESeq2 v1.14.1 [80].

**Small RNA library analysis** Reads were trimmed of 3’ adapter sequences with cutadapt v1.10 [81] (-m 15 -a TGAATTCTCGGGTGCCAAGG). Trimmed reads were aligned to the mouse genome reference sequence (mm10), masked for NUMTs regions, with bowtie2 [76], and the subsequent alignments filtered with SAMtools v1.3.1 [77] (-q 2 -F 260) to exclude unmapped reads, secondary alignments, and multireads. Mitochondrial alignments were extracted and split by strand, and coverage was calculated with BEDtools [78] genomcov (-d -scale [1e+06/total mapped

reads]), normalized to the total number of mapped reads to the mouse whole genome (reads per million; RPM), and converted to wig format for visualization. Gene-level counts for the nuclear genome were calculated with featureCounts [79] (-s 1), while counts for mitochondrial genes were calculated with BEDtools coverage (-counts -s -F 0.80). Count tables were collated in R v3.3.2 [74], and differential expression between conditions was analyzed with DESeq2 v1.14.1 [80].

### Statistical analysis

Experiments were performed at least three times, and results are representative of  $n > 5$  independent biological replicates, unless indicated otherwise. All values are expressed as means  $\pm$  SEM. Statistical analysis of proteomics and RNA sequencing are described above. Other statistical analyses were conducted using GraphPad Prism 5 software. Statistical significance between two groups was assessed by two-tailed unpaired Student's *t*-test, and statistical significance between more than two groups was performed using one-way analysis of variance (ANOVA). Differences were considered statistically significant at a value of  $P < 0.05$ .

### Data availability

The RNA sequencing data have uploaded to GEO database, with the access number of GSE102255. The mass spectrometry proteomics data have been deposited to the ProteomeXchange Consortium via the PRIDE [82] partner repository with the dataset identifier PXD013398.

**Expanded View** for this article is available online.

### Acknowledgements

We thank Maria Falkenberg, Christoph Freyer, and Paula Clemente for technical suggestions and critical input, and Thomas J. Nicholls and Susanne Viriding for technical assistance. We are also grateful for the technical support from the Proteomics Core Facility, Max Planck Institute for Biology of Ageing; in particular, we acknowledge Xiping Li. RNA library construction and sequencing were performed at the Cologne Center for Genomics. This work was supported by the Knut och Alice Wallenbergs Stiftelse (Knut and Alice Wallenberg Foundation), Swedish Research Council: 2015-00418, Novo Nordisk Fonden and the Max Planck Society to N.-G. Larsson. A. Filipovska receives support from the Australian Research Council (DP170103000) and the National Health and Medical Research Council of Australia (APP1067837 and APP1058442).

### Author contributions

SJ, CK, and N-GL conceived the project, designed the experiments, and wrote the manuscript. SJ performed and interpreted the majority of the experiments. SJ, CK, N-GL, IK, and MM advised on methodology and interpreted the data. JM, SS, IK, ESR, MM, MJ, OL, IA, FAS, VP, RW, and KH performed experiments and analyzed the data. DM, AF, and CMG contributed on experiment design, interpreted the data, and edited the manuscript. N-GL supervised the project. All the authors commented on the manuscript.

### Conflict of interest

The authors declare that they have no conflict of interest.

## References

- Wallace DC (1999) Mitochondrial diseases in man and mouse. *Science* 283: 1482–1488
- Larsson N-G (2010) Somatic mitochondrial DNA mutations in mammalian aging. *Annu Rev Biochem* 79: 683–706
- Kaupilla TES, Kaupilla JHK, Larsson N-G (2017) Mammalian mitochondria and aging: an update. *Cell Metab* 25: 57–71
- Scarpulla RC (2008) Transcriptional paradigms in mammalian mitochondrial biogenesis and function. *Physiol Rev* 88: 611–638
- Gustafsson CM, Falkenberg M, Larsson N-G (2016) Maintenance and expression of mammalian mitochondrial DNA. *Annu Rev Biochem* 85: 133–160
- Clayton DA (1991) Replication and transcription of vertebrate mitochondrial DNA. *Annu Rev Cell Biol* 7: 453–478
- Chang DD, Clayton DA (1987) A novel endoribonuclease cleaves at a priming site of mouse mitochondrial DNA replication. *EMBO J* 6: 409–417
- Falkenberg M, Larsson N-G, Gustafsson CM (2007) DNA replication and transcription in mammalian mitochondria. *Annu Rev Biochem* 76: 679–699
- Falkenberg M, Gaspari M, Rantanen A, Trifunovic A, Larsson N-G, Gustafsson CM (2002) Mitochondrial transcription factors B1 and B2 activate transcription of human mtDNA. *Nat Genet* 31: 289–294
- Ringel R, Sologub M, Morozov YI, Litonin D, Cramer P, Temiakov D (2011) Structure of human mitochondrial RNA polymerase. *Nature* 478: 269–273
- Kühl I, Miranda M, Posse V, Milenkovic D, Mourier A, Siira SJ, Bonekamp NA, Neumann U, Filipovska A, Polosa PL et al (2016) POLRMT regulates the switch between replication primer formation and gene expression of mammalian mtDNA. *Sci Adv* 2: e1600963
- Posse V, Hoberg E, Dierckx A, Shahzad S, Koolmeister C, Larsson N-G, Wilhelmsson LM, Hällberg BM, Gustafsson CM (2014) The amino terminal extension of mammalian mitochondrial RNA polymerase ensures promoter specific transcription initiation. *Nucleic Acids Res* 42: 3638–3647
- Morozov YI, Agaronyan K, Cheung ACM, Anikin M, Cramer P, Temiakov D (2014) A novel intermediate in transcription initiation by human mitochondrial RNA polymerase. *Nucleic Acids Res* 42: 3884–3893
- Mangus DA, Jang SH, Jaehning JA (1994) Release of the yeast mitochondrial RNA polymerase specificity factor from transcription complexes. *J Biol Chem* 269: 26568–26574
- Sologub M, Litonin D, Anikin M, Mustaev A, Temiakov D (2009) TFB2 is a transient component of the catalytic site of the human mitochondrial RNA polymerase. *Cell* 139: 934–944
- Minczuk M, He J, Duch AM, Ettema TJ, Chlebowski A, Dzionek K, Nijtmans LGJ, Huynen MA, Holt IJ (2011) TEFM (c17orf42) is necessary for transcription of human mtDNA. *Nucleic Acids Res* 39: 4284–4299
- Posse V, Shahzad S, Falkenberg M, Hällberg BM, Gustafsson CM (2015) TEFM is a potent stimulator of mitochondrial transcription elongation *in vitro*. *Nucleic Acids Res* 43: 2615–2624
- Hillen HS, Morozov YI, Sarfallah A, Temiakov D, Cramer P (2017) Structural basis of mitochondrial transcription initiation. *Cell* 171: 1072–1081.e10
- Hillen HS, Parshin AV, Agaronyan K, Morozov YI, Graber JJ, Chernev A, Schwinghammer K, Urlaub H, Anikin M, Cramer P et al (2017) Mechanism of transcription anti-termination in human mitochondria. *Cell* 171: 1082–1093.e13

20. Yu H, Xue C, Long M, Jia H, Xue G, Du S, Coello Y, Ishibashi T (2018) TEFM enhances transcription elongation by modifying mtRNAP pausing dynamics. *Biophys J* 115: 2295–2300
21. Pham XH, Farge G, Shi Y, Gaspari M, Gustafsson CM, Falkenberg M (2006) Conserved sequence box II directs transcription termination and primer formation in mitochondria. *J Biol Chem* 281: 24647–24652
22. Wanrooij PH, Uhler JP, Simonsson T, Falkenberg M, Gustafsson CM (2010) G-quadruplex structures in RNA stimulate mitochondrial transcription termination and primer formation. *Proc Natl Acad Sci USA* 107: 16072–16077
23. Wanrooij PH, Uhler JP, Shi Y, Westerlund F, Falkenberg M, Gustafsson CM (2012) A hybrid G-quadruplex structure formed between RNA and DNA explains the extraordinary stability of the mitochondrial R-loop. *Nucleic Acids Res* 40: 10334–10344
24. Lee DY, Clayton DA (1996) Properties of a primer RNA-DNA hybrid at the mouse mitochondrial DNA leading-strand origin of replication. *J Biol Chem* 271: 24262–24269
25. Xu B, Clayton DA (1995) A persistent RNA-DNA hybrid is formed during transcription at a phylogenetically conserved mitochondrial DNA sequence. *Mol Cell Biol* 15: 580–589
26. Xu B, Clayton DA (1996) RNA-DNA hybrid formation at the human mitochondrial heavy-strand origin ceases at replication start sites: an implication for RNA-DNA hybrids serving as primers. *EMBO J* 15: 3135–3143
27. Agaronyan K, Morozov YI, Anikin M, Temiakov D (2015) Mitochondrial biology. Replication-transcription switch in human mitochondria. *Science* 347: 548–551
28. Reinhard L, Sridhara S, Hällberg BM (2017) The MRPP1/MRPP2 complex is a tRNA-maturation platform in human mitochondria. *Nucleic Acids Res* 45: 12469–12480
29. Jourdain AA, Koppen M, Wydro M, Rodley CD, Lightowlers RN, Chrzanoska-Lightowlers ZM, Martinou J-C (2013) GRSF1 regulates RNA processing in mitochondrial RNA granules. *Cell Metab* 17: 399–410
30. Antonicka H, Sasarman F, Nishimura T, Paupe V, Shoubridge EA (2013) The mitochondrial RNA-binding protein GRSF1 localizes to RNA granules and is required for posttranscriptional mitochondrial gene expression. *Cell Metab* 17: 386–398
31. Pearce SF, Rebelo-Guiomar P, D'Souza AR, Powell CA, Van Haute L, Minczuk M (2017) Regulation of mammalian mitochondrial gene expression: recent advances. *Trends Biochem Sci* 42: 625–639
32. Ojala D, Montoya J, Attardi G (1981) tRNA punctuation model of RNA processing in human mitochondria. *Nature* 290: 470–474
33. Holzmann J, Frank P, Löffler E, Bennett KL, Gerner C, Rossmannith W (2008) RNase P without RNA: identification and functional reconstitution of the human mitochondrial tRNA processing enzyme. *Cell* 135: 462–474
34. Rackham O, Busch JD, Matic S, Siira SJ, Kuznetsova I, Atanassov I, Ermer JA, Shearwood A-MJ, Richman TR, Stewart JB et al (2016) Hierarchical RNA processing is required for mitochondrial ribosome assembly. *Cell Rep* 16: 1874–1890
35. Brzezniak LK, Bijata M, Szczesny RJ, Stepień PP (2011) Involvement of human ELAC2 gene product in 3' end processing of mitochondrial tRNAs. *RNA Biol* 8: 616–626
36. Siira SJ, Rossetti G, Richman TR, Perks K, Ermer JA, Kuznetsova I, Hughes L, Shearwood A-MJ, Viola HM, Hool LC et al (2018) Concerted regulation of mitochondrial and nuclear non-coding RNAs by a dual-targeted RNase Z. *EMBO Rep* 19: e46198
37. Bogenhagen DF, Martin DW, Koller A (2014) Initial steps in RNA processing and ribosome assembly occur at mitochondrial DNA nucleoids. *Cell Metab* 19: 618–629
38. Pietras Z, Wojcik MA, Borowski LS, Szewczyk M, Kulinski TM, Cysewski D, Stepień PP, Dziembowski A, Szczesny RJ (2018) Dedicated surveillance mechanism controls G-quadruplex forming non-coding RNAs in human mitochondria. *Nat Commun* 9: 2558
39. Antonicka H, Shoubridge EA (2015) Mitochondrial RNA granules are centers for posttranscriptional RNA processing and ribosome biogenesis. *Cell Rep* 10: 920–932
40. Jourdain AA, Koppen M, Rodley CD, Maundrell K, Gueguen N, Reynier P, Guaras AM, Enriquez JA, Anderson P, Simarro M et al (2015) A mitochondria-specific isoform of FASTK is present in mitochondrial RNA granules and regulates gene expression and function. *Cell Rep* 10: 1110–1121
41. Wilson WC, Hornig-Do H-T, Bruni F, Chang JH, Jourdain AA, Martinou J-C, Falkenberg M, Spähr H, Larsson N-G, Lewis RJ et al (2014) A human mitochondrial poly(A) polymerase mutation reveals the complexities of post-transcriptional mitochondrial gene expression. *Hum Mol Genet* 23: 6345–6355
42. Lee K-W, Okot-Kotber C, LaComb JF, Bogenhagen DF (2013) Mitochondrial ribosomal RNA (rRNA) methyltransferase family members are positioned to modify nascent rRNA in foci near the mitochondrial DNA nucleoid. *J Biol Chem* 288: 31386–31399
43. Borowski LS, Dziembowski A, Hejnowicz MS, Stepień PP, Szczesny RJ (2013) Human mitochondrial RNA decay mediated by PNase-hSuv3 complex takes place in distinct foci. *Nucleic Acids Res* 41: 1223–1240
44. Larsson NG, Wang J, Wilhelmsson H, Oldfors A, Rustin P, Lewandoski M, Barsh GS, Clayton DA (1998) Mitochondrial transcription factor A is necessary for mtDNA maintenance and embryogenesis in mice. *Nat Genet* 18: 231–236
45. Ruzzenente B, Metodiev MD, Wredenberg A, Bratic A, Park CB, Cámara Y, Milenkovic D, Zickermann V, Wibom R, Hulthenby K et al (2012) LRRPRC is necessary for polyadenylation and coordination of translation of mitochondrial mRNAs. *EMBO J* 31: 443–456
46. Milenkovic D, Matic S, Kühl I, Ruzzenente B, Freyer C, Jemt E, Park CB, Falkenberg M, Larsson N-G (2013) TWINKLE is an essential mitochondrial helicase required for synthesis of nascent D-loop strands and complete mtDNA replication. *Hum Mol Genet* 22: 1983–1993
47. Cámara Y, Asin-Cayuela J, Park CB, Metodiev MD, Shi Y, Ruzzenente B, Kukut C, Habermann B, Wibom R, Hulthenby K et al (2011) MTERF4 regulates translation by targeting the methyltransferase NSUN4 to the mammalian mitochondrial ribosome. *Cell Metab* 13: 527–539
48. Smeitink J, van den Heuvel L, DiMauro S (2001) The genetics and pathology of oxidative phosphorylation. *Nat Rev Genet* 2: 342–352
49. Metodiev MD, Lesko N, Park CB, Cámara Y, Shi Y, Wibom R, Hulthenby K, Gustafsson CM, Larsson N-G (2009) Methylation of 12S rRNA is necessary for *in vivo* stability of the small subunit of the mammalian mitochondrial ribosome. *Cell Metab* 9: 386–397
50. Wredenberg A, Wibom R, Wilhelmsson H, Graff C, Wiener HH, Burden SJ, Oldfors A, Westerblad H, Larsson N-G (2002) Increased mitochondrial mass in mitochondrial myopathy mice. *Proc Natl Acad Sci USA* 99: 15066–15071
51. Wibom R, Hagenfeldt L, von Döbeln U (2002) Measurement of ATP production and respiratory chain enzyme activities in mitochondria isolated from small muscle biopsy samples. *Anal Biochem* 311: 139–151
52. Park CB, Asin-Cayuela J, Cámara Y, Shi Y, Pellegrini M, Gaspari M, Wibom R, Hulthenby K, Erdjument-Bromage H, Tempst P et al (2007) MTERF3 is a negative regulator of mammalian mtDNA transcription. *Cell* 130: 273–285



53. Calvo SE, Clauser KR, Mootha VK (2016) MitoCarta2.0: an updated inventory of mammalian mitochondrial proteins. *Nucleic Acids Res* 44: D1251–D1257
54. Kühl I, Miranda M, Atanassov I, Kuznetsova I, Hinze Y, Mourier A, Filipovska A, Larsson N-G (2017) Transcriptomic and proteomic landscape of mitochondrial dysfunction reveals secondary coenzyme Q deficiency in mammals. *Elife* 6: e30952
55. Chang DD, Hauswirth WW, Clayton DA (1985) Replication priming and transcription initiate from precisely the same site in mouse mitochondrial DNA. *EMBO J* 4: 1559–1567
56. Roux KJ, Kim DI, Burke B (2013) BioID: a screen for protein-protein interactions. *Curr Protoc Protein Sci* 74: Unit19.23–19.23.14
57. Jourdain AA, Boehm E, Maundrell K, Martinou J-C (2016) Mitochondrial RNA granules: compartmentalizing mitochondrial gene expression. *J Cell Biol* 212: 611–614
58. Matic S, Jiang M, Nicholls TJ, Uhler JP, Dirksen-Schwanenland C, Polosa PL, Simard M-L, Li X, Atanassov I, Rackham O et al (2018) Mice lacking the mitochondrial exonuclease MGME1 accumulate mtDNA deletions without developing progeria. *Nat Commun* 9: 1202
59. Dong DW, Pereira F, Barrett SP, Kolesar JE, Cao K, Damas J, Yatsunyk LA, Johnson FB, Kaufman BA (2014) Association of G-quadruplex forming sequences with human mtDNA deletion breakpoints. *BMC Genom* 15: 677
60. Bharti SK, Sommers JA, Zhou J, Kaplan DL, Spelbrink JN, Mergny J-L, Brosh RM (2014) DNA sequences proximal to human mitochondrial DNA deletion breakpoints prevalent in human disease form G-quadruplexes, a class of DNA structures inefficiently unwound by the mitochondrial replicative Twinkle helicase. *J Biol Chem* 289: 29975–29993
61. Huang W-C, Tseng T-Y, Chen Y-T, Chang C-C, Wang Z-F, Wang C-L, Hsu T-N, Li P-T, Chen C-T, Lin J-J et al (2015) Direct evidence of mitochondrial G-quadruplex DNA by using fluorescent anti-cancer agents. *Nucleic Acids Res* 43: 10102–10113
62. Tornaletti S, Park-Snyder S, Hanawalt PC (2008) G4-forming sequences in the non-transcribed DNA strand pose blocks to T7 RNA polymerase and mammalian RNA polymerase II. *J Biol Chem* 283: 12756–12762
63. Bentley DL (2014) Coupling mRNA processing with transcription in time and space. *Nat Rev Genet* 15: 163–175
64. Kolasinska-Zwierz P, Down T, Latorre I, Liu T, Liu XS, Ahringer J (2009) Differential chromatin marking of introns and expressed exons by H3K36me3. *Nat Genet* 41: 376–381
65. Posse V, Al-Behadili A, Uhler JP, Clausen AR, Reyes A, Zeviani M, Falkenberg M, Gustafsson CM (2019) RNase H1 directs origin-specific initiation of DNA replication in human mitochondria. *PLoS Genet* 15: e1007781
66. Dasgupta S, Masukata H, Tomizawa J (1987) Multiple mechanisms for initiation of ColE1 DNA replication: DNA synthesis in the presence and absence of ribonuclease H. *Cell* 51: 1113–1122
67. Surovtseva YV, Shutt TE, Cotney J, Cimen H, Chen SY, Koc EC, Shadel GS (2011) Mitochondrial ribosomal protein L12 selectively associates with human mitochondrial RNA polymerase to activate transcription. *Proc Natl Acad Sci USA* 108: 17921–17926
68. Nouws J, Goswami AV, Bestwick M, McCann BJ, Surovtseva YV, Shadel GS (2016) Mitochondrial ribosomal protein L12 is required for POLRMT stability and exists as two forms generated by alternative proteolysis during import. *J Biol Chem* 291: 989–997
69. Rappsilber J, Ishihama Y, Mann M (2003) Stop and go extraction tips for matrix-assisted laser desorption/ionization, nanoelectrospray, and LC/MS sample pretreatment in proteomics. *Anal Chem* 75: 663–670
70. Cox J, Mann M (2008) MaxQuant enables high peptide identification rates, individualized p.p.b.-range mass accuracies and proteome-wide protein quantification. *Nat Biotechnol* 26: 1367–1372
71. Cox J, Neuhauser N, Michalski A, Scheltema RA, Olsen JV, Mann M (2011) Andromeda: a peptide search engine integrated into the MaxQuant environment. *J Proteome Res* 10: 1794–1805
72. Cox J, Hein MY, Luber CA, Paron I, Nagaraj N, Mann M (2014) Accurate proteome-wide label-free quantification by delayed normalization and maximal peptide ratio extraction, termed MaxLFQ. *Mol Cell Proteomics* 13: 2513–2526
73. Tyanova S, Temu T, Sinitcyn P, Carlson A, Hein MY, Geiger T, Mann M, Cox J (2016) The Perseus computational platform for comprehensive analysis of (prote)omics data. *Nat Methods* 13: 731–740
74. Dalgaard P, R Development Core Team (2010) *R: a language and environment for statistical computing*. Vienna, Austria: R Development Core Team. Computer programme, Retrieved from <http://www.R-project.org/>
75. Ritchie ME, Phipson B, Wu D, Hu Y, Law CW, Shi W, Smyth GK (2015) limma powers differential expression analyses for RNA-sequencing and microarray studies. *Nucleic Acids Res* 43: e47–e47
76. Langmead B, Salzberg SL (2012) Fast gapped-read alignment with Bowtie 2. *Nat Methods* 9: 357–359
77. Li H, Handsaker B, Wysoker A, Fennell T, Ruan J, Homer N, Marth G, Abecasis G, Durbin R, 1000 Genome Project Data Processing Subgroup (2009) The sequence alignment/Map format and SAMtools. *Bioinformatics* 25: 2078–2079
78. Quinlan AR, Hall IM (2010) BEDTools: a flexible suite of utilities for comparing genomic features. *Bioinformatics* 26: 841–842
79. Liao Y, Smyth GK, Shi W (2014) featureCounts: an efficient general purpose program for assigning sequence reads to genomic features. *Bioinformatics* 30: 923–930
80. Love MI, Huber W, Anders S (2014) Moderated estimation of fold change and dispersion for RNA-seq data with DESeq2. *Genome Biol* 15: 550
81. Martin M (2011) Cutadapt removes adapter sequences from high-throughput sequencing reads. *EMBnet J* 17: 10–12
82. Perez-Riverol Y, Csordas A, Bai J, Bernal-Llinares M, Hewapathirana S, Kundu DJ, Inuganti A, Griss J, Mayer G, Eisenacher M et al (2019) The PRIDE database and related tools and resources in 2019: improving support for quantification data. *Nucleic Acids Res* 47: D442–D450



**License:** This is an open access article under the terms of the Creative Commons Attribution-NonCommercial-NoDerivs 4.0 License, which permits use and distribution in any medium, provided the original work is properly cited, the use is non-commercial and no modifications or adaptations are made.